MASTER THESIS

Investigations on telescope yielding elements with porous filling

BSc Marko Verient

Institute for Rock Mechanics and Tunnelling
Graz University of Technology

Advisors:

O.Univ.-Prof. Dipl.-Ing. Dr.mont. Wulf Schubert

Institute for Rock Mechanics and Tunnelling
Graz University of Technology

Dipl.-Ing. Alexander Kluckner

Institute for Rock Mechanics and Tunnelling
Graz University of Technology

Graz, November 2014

STATUTORY DECLARATION

I declare that I have authored this thesis independently, that I have not used other than the declared sources / resources, and that I have explicitly marked all material which has been quoted either literally or by content from the used sources. The text document uploaded to TUGRAZonline is identical to the present master thesis.

Graz, November 2014

_____

Marko Verient

Acknowledgements (Danksagung)

Abstract

Tunnelling in weak ground and under high overburden always proves to be challenging during the design and construction phase. Currently tunnels are constructed with increasing lengths, which increases the probability of crossing tectonic fault zones under high overburden. These geological conditions are commonly associated with high loads and massive deformation of the lining.

The idea of using high ductile elements in the lining has become a well-known practise in above-mentioned conditions. During the last century, different solutions have been developed.

In this thesis the main focus is on the Telescope-Yielding-Elements (TSR).
The big advantage of these elements is that force-oscillation can be reduced to an insignificantly low level and the deformation behaviour can be controlled by the use of porous fillings, different steel pipes and additional free space.

Kurzfassung

Um die auftretenden Verformungen im Gebirge zu kompensieren wurden verschiedenste Stauchelemente entwickelt. Eines dieser Elemente ist der "Lining Stress Controler" (LSC) der am Institut für Felsmechanik und Tunnelbau an der Technischen Universität Graz entwickelt wurde. Als Weiterentwicklung dieses Typs von Stauchelementen wurde das "Teleskop Stauchrohr" (TSR) entwickelt, worum es in dieser Arbeit hautsächlich geht.

Durch das Beulen der LSC´s entsteht eine Oszillation der Widerstandskraft der Elemente. Um dies zu minimieren wurden Versuche mit gefüllten LSC´s durchgeführt. Als Füllung wurde eine zementgebundene poröse Füllung verwendet.

Bei den TSR kam es zu beinahe gar keiner Oszillation der Arbeitslinie. Das Problem war der begrenzte Stauchweg. Durch zusätzlichen Hohlraum, Optimierung des Füllers und der inneren und äußeren Stahlrohre wurde in dieser Arbeit versucht, das Teleskop Stauchrohr zu optimieren.

Contents

Figures

Tables

Abbreviations

LSC	…………..	*Lining Stress Controller*
TSR	…………..	Telescope-Yielding-Element
UCS	…………..	Uniaxial Compressive Strength
GRC	…………..	Ground Reaction Curve

Symbols

$A; B$	$[1/dMPa]$	constants
a	$[m/d]$	advance rate
$C_1; C_2$	$[-]$	coefficient
$\overline{C_1}; \overline{C_2}$	$[-]$	coefficient
c	$[MPa]$	ground cohesion
$C_{d\infty}$	$[1/MPa]$	flow-rate creep parameter
$C_{(t)}$	$[1/MPa]$	time-dependent plastic creep rate
$\Delta C_{(t)}$	$[-]$	increment of time-dependent plastic creep rate
E	$[MPa]$	Young's modulus of the ground
$E_{(t)}$	$[MPa]$	time-dependent Young's modulus
E_{28}	$[MPa]$	secant modulus of shotcrete at age of 28 days
K_u	$[-]$	coefficient
p_a	$[MPa]$	support pressure
p_k	$[MPa]$	yield strength of the ground according to the Mohr-Coulomb failure criterion
p_i	$[MPa]$	primary stress
$^S p_i$	$[MPa]$	asymmetric part of primary stress
$^A p_i$	$[MPa]$	symmetric part of primary stress
$p_{k,pl}$	$[MPa]$	plastic (post-failure) yield strength of the ground
$p_{k,el}$	$[MPa]$	elastic (pre-failure) yield strength of the ground
Q	$[1/MPa]$	low-rate creep parameter
r	$[m]$	radius
R_0	$[m]$	tunnel radius
$\tilde{R}$	$[m]$	radius of the plastic zone
$\bar{R}$	$[m]$	radius where the tangential stress equals the vertical primary stress
t	$[day]$	time
$u(x)$	$[m]$	radial displacements at the face distance x
u_f	$[m]$	pre-displacements
$u_{\tilde{R}}$	$[m]$	radial displacements
u_∞	$[m]$	final radial displacements
σ_r	$[MPa]$	radial stress
$\sigma_{r\tilde{R}}$	$[MPa]$	radial stress at the boundary of the failure zone
$\sigma_{r,pl}$	$[MPa]$	plastic radial stress
$\sigma_{\vartheta,pl}$	$[MPa]$	plastic tangential stress

$\sigma_{\vartheta\tilde{R}}$	$[MPa]$	tangential stress at the boundary of the failure zone
$\sigma_{r,el}$	$[MPa]$	elastic radial stress
$\sigma_{\vartheta,el}$	$[MPa]$	elastic tangential stress
σ_2	$[MPa]$	axial stress at the end of the second time interval
ε_1	$[-]$	axial strain at the time "1" (begin of interval)
ε_2	$[-]$	axial strain at the time "2" (end of interval)
$\Delta\varepsilon_d$	$[-]$	increment of reversible creep strain
ε_d	$[-]$	reversible creep strain
$\Delta\varepsilon_{sh}$	$[-]$	increment of shrinkage strain
ε_{sh}	$[-]$	shrinkage strain
$\varepsilon_{sh\,\infty}$	$[-]$	final shrinkage strain of shotcrete
α	$[-]$	factor for volume expansion (dilation) due to ground failure
β_{gd}	$[MPa]$	unaxial compressive strength of the ground
λ_p	$[-]$	coefficient of passive lateral pressure
$\lambda_{p,pl}$	$[-]$	plastic coefficient of passive lateral pressure
$\lambda_{p,el}$	$[-]$	elastic coefficient of passive lateral pressure
φ	$[°]$	friction angle of the ground
φ_{pl}	$[°]$	plastic friction angle
φ_{el}	$[°]$	elastic friction angle
ν	$[-]$	Poisson's ratio
ψ	$[°]$	angle in circumferential direction starting from the crown

1 Introduction

Tunnelling in weak ground and under high overburden always proves to be challenging during the design and construction phase. Current tunnels are constructed with increasing lengths, which increases the probability of crossing tectonic fault zones under high overburden. These geological conditions are commonly associated with high loads and massive deformation of the lining. Conventional linings have a tendency to suffer considerable damage under those high loads, which subsequently leads to significant repair costs.

To avoid these costs and protect the lining from damage, the idea of using highly ductile elements in the lining has become a well-known practise in above-mentioned conditions. During the last decades different solutions (e.g. yielding elements like Lining Stress Controller (Moritz, 1999), WABE System (Eisenhütte Bochum) or hiDCon (Solexperts)) have been developed to mitigate the adverse effect those high deformations are prone to have on the shotcrete lining (Radončić, 2011).

Maximum displacement rates usually occur close behind the tunnel face, where the young shotcrete offers still has a low strength. Therefore, a yielding element with similar low stiffness at the beginning of the deformations is required to protect the young shotcrete. With increasing stiffness of the shotcrete lining, the stiffness of the yielding elements should increase as well. The ideal result would be a characteristic yielding-element curve that follows the characteristic time-dependant curve of the shotcrete capacity with respect to the advance rate and the stress regime, prevailing on site.

In 2011, Radončić and Sitzwohl conducted lab trials on Lining Stress Controllers (LSC) at the Institute for Rock Mechanics and Tunnelling, Graz University of Technology. The lab results are documented in the master thesis of (Sitzwohl, 2011). This thesis also provides an overview of the various yielding elements that are in common use nowadays. While conducting these tests, the principles of the Telescope-Yielding-Elements (TSR) were specified representing a further development of the LSC (Sitzwohl, 2011; Radončić, 2011). The big advantage of the TSR elements is that force-oscillation can be reduced to an insignificantly low level and the deformation behaviour can be controlled by the use of porous fillings.

1.1 Aim of the thesis

The focus of this work lies in the optimization of the Telescope-yielding-elements (TSR) with a porous filling (Figure 1-1) including tests in the lab. The work covers following steps:

- For the identification of the ideal-characteristic-curve for the yielding elements, a program has to be written in MATLAB.
- Investigations on the filling. The shape and mixture of the porous filling should be as simple as possible, to achieve a fast manufacturing process.
- Investigations on the shuttering for the filling. A cheap shuttering-system with high efficiency and an appropriate shape has to be found and tested.
- Conduct tests on Telescope-yielding-elements with different settings and new filling mixtures.
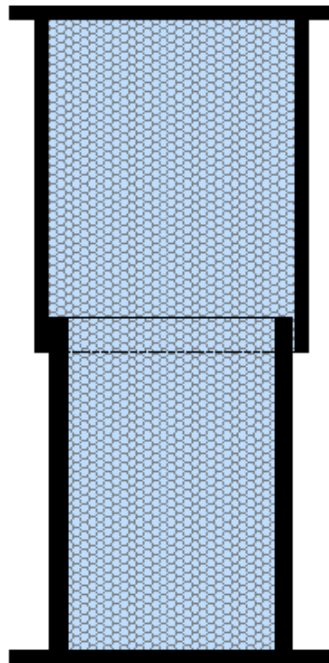
Figure 1-1: Telescope-yielding-element with porous filling.

The stress-strain behaviour of the TSR obtained in the lab is then compared with the ideal-characteristic-curve derived from MATLAB. The MATLAB program includes varying properties for the rock mass and the rheological behaviour of the shotcrete.

2 Requirements on yielding elements

The utilization of the shotcrete lining is amongst others directly linked to the time-dependent behaviour of the shotcrete and the displacement development of the rock mass. However, for the purposes of this study, full-face excavation was considered and influence of additional support material (e.g. bolts) was neglected. To include the influence of boundary conditions not considered here (sequential excavation, non-hydrostatic stress regime, etc.), the maximum utilization of the shotcrete lining was limited with 80% of its capacity.

To arrive at an ideal load-displacement characteristic of the yielding elements, a MATLAB program was developed.

For the determination of this curve, the following interactions have to be considered

- Time and force depending rheological behaviour of the shotcrete
- Displacement development in relation to the face distance
- Advance rate
- Geometry of the shotcrete lining (number of gaps for the yielding elements, thickness of shotcrete)

The input parameters are shown in Table 1. The used formulas are summarized in the Appendix B (see page 58).

Table 1: Input parameters for the MATLAB program.

Tunnel radius [m]	R_0
Advance rate [m] per day	a
Elastic friction angle rock mass [°]	φ_{el}
Plastic friction angle rock mass [°]	φ_{pl}
Elastic cohesion rock mass [MPa]	c_{el}
Plastic cohesion rock mass [MPa]	c_{pl}
Young´s modulus rock mass [MPa]	E
Poisson ratio rock mass [-]	ν
Primary stress [MPa]	p_i
Number of LSC gaps in cross section [-]	num_{LSC}
LSC height [m]	len_{LSC}
Thickness of shotcrete lining [m]	d_{shot}
Utilization of the shotcrete lining [-]	cap_{shot}
Flow-rate creep parameter [-]	$C_{d\infty}$

Final shrinkage strain of shotcrete [-]	$\varepsilon_{sh\,\infty}$
Secant modulus of shotcrete at age of 28 days [MPa]	E_{28}
Constant A [-]	A
Constant B [-]	B
Constant Q [-]	Q
Constant s [-]	s
Constant n [-]	n
UCS of shotcrete after 28 days [MPa]	σ_{28}
Factor for volume expansion [-]	α
Number of decompression steps for the GRC [-]	num_{step}
Maximal face distance [m]	d_{Face}
Installation of shotcrete lining [days]	t_{offset}

2.1 Stress-strain curve

2.1.1 Example

Figure 2-2 shows two characteristic curves. For a specific tunnel project encountering different rock mass conditions, the upper curve relates to tunnel sections with higher rock mass quality, whereas the lower curve relates to sections with lower rock mass quality. The parameters are shown in Table 2. The trend of the curve includes the time depend shotcrete hardening (Schubert, 1988), and a maximal load capacity (for example 80%), so the shotcrete is not damaged.

Table 2: Example Input parameters for the MATLAB program.

		Upper curve	Lower curve
Tunnel radius [m]	R_0	5	5
Advance rate [m] per day	a	4	4
Elastic friction angle rock mass [°]	φ_{el}	30	28
Plastic friction angle rock mass [°]	φ_{pl}	28	26
Elastic cohesion rock mass [MPa]	c_{el}	0.4	0.3
Plastic cohesion rock mass [MPa]	c_{pl}	0.2	0.2
Young´s modulus rock mass [MPa]	E	5500	2500
Poisson's ratio rock mass [-]	ν	0.25	0.3
Primary stress [MPa]	p_i	15	10
Number of LSC gaps in cross section [-]	gap_{LSC}	4	5
LSC height [m]	len_{LSC}	0.4	0.4
Thickness of shotcrete lining [m]	d_{shot}	0.3	0.25
Utilization of the shotcrete lining [-]	cap_{shot}	0.8	0.8
Flow-rate creep parameter [-]	$C_{d\infty}$	0.00009	0.00009
Final shrinkage strain of shotcrete [-]	$\varepsilon_{sh\,\infty}$	0.00125	0.00125
Secant modulus of shotcrete at age of 28 days [MPa]	E_{28}	15000	15000
Constant A [-]	A	0.0001	0.0001
Constant B [-]	B	600	600
Constant Q [-]	Q	0.0001	0.0001
Constant s [-]	s	0.2	0.2
Constant n [-]	n	0.5	0.5
UCS of shotcrete after 28 days [MPa]	σ_{28}	40	30
Factor for volume expansion [-]	α	1	1
Number of decompression steps for the GRC [-]	num_{step}	100	100
Maximal face distance [m]	d_{Face}	100	100
Installation of shotcrete lining [days]	t_{offset}	0.1667	0.16667
Yielding elements per gap and meter	num_{LSC}	3	3
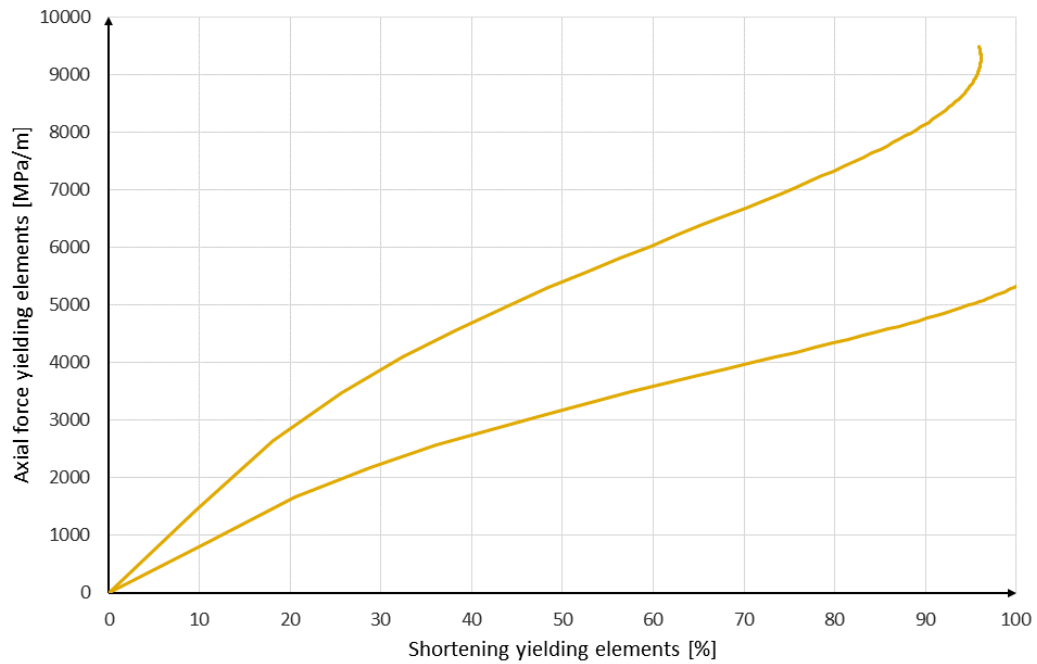
Figure 2-1: Upper and lower limit of an ideal-characteristic-curve from the MATLAB program.

After installation, shotcrete has a low strength, requiring also a low resistance of the yielding elements. With elapsing time, as the shotcrete hardens, the yielding elements should also provide more resistance. The design of the telescope-yielding-elements should be in a way to meet these requirements.

Figure 2-2 show almost the same as shown in Figure 2-1. The difference is that the figure below shows a simplified ideal-characteristic-area, which we want to achieve with our test results.
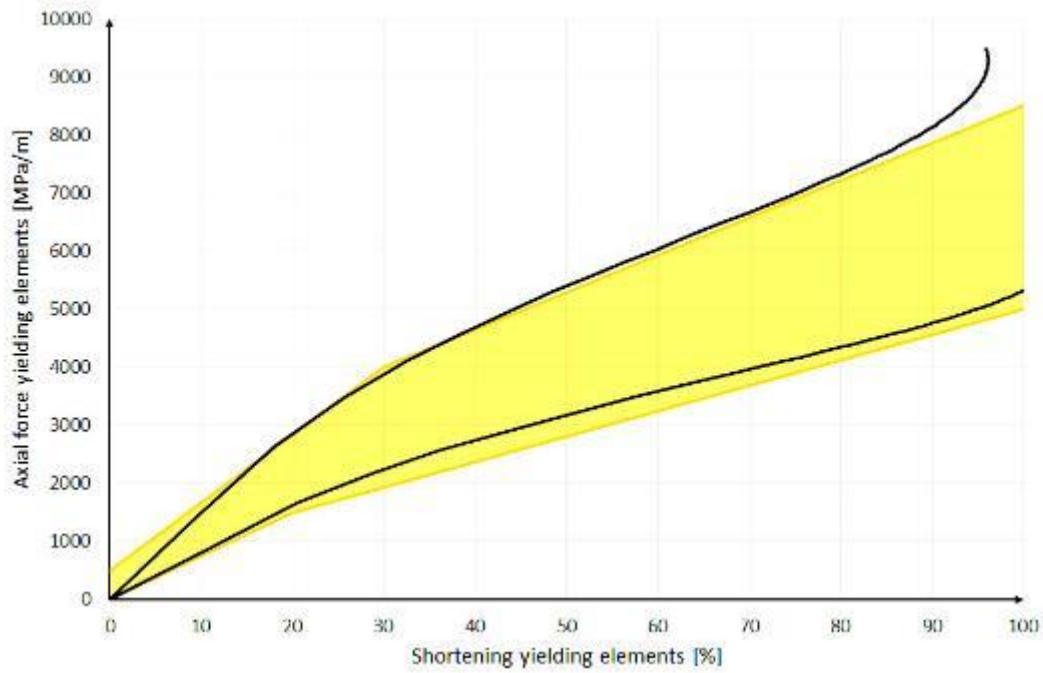
Figure 2-2: The ideal-characteristic-area of yielding element per meter.

Figure 2-3 shows the same as in Figure 2-2, with the difference that the diagram below show the area for one single yielding element. This area is the indication for our laboratory tests.
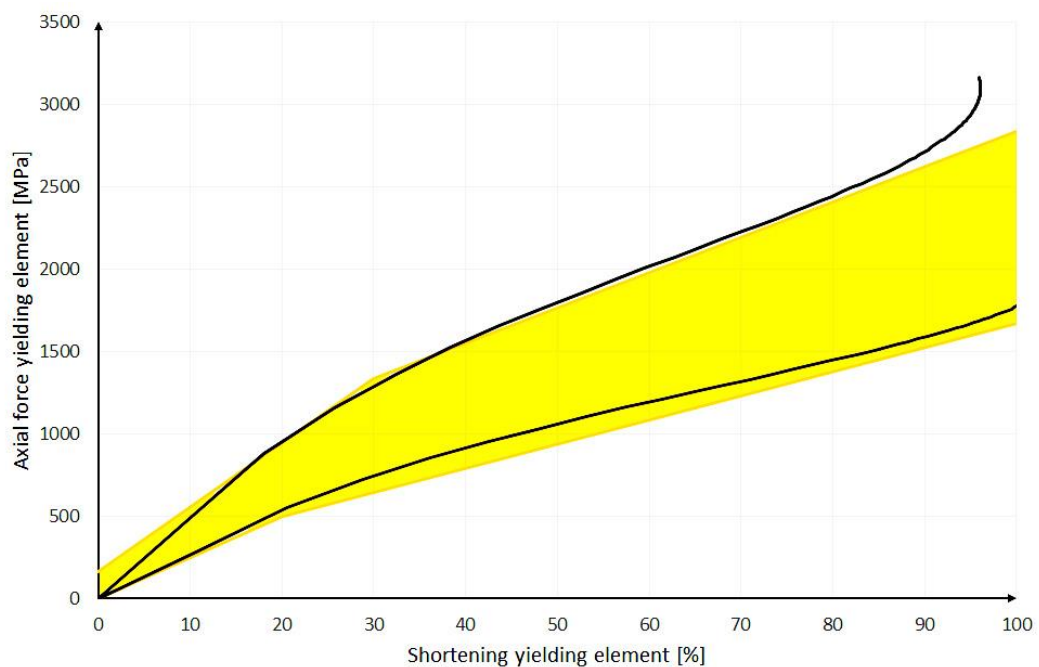
Figure 2-3: The ideal-characteristic-area for one single element.

2.1 General description of the TSR

2.1.1 Basic setup

The basic arrangement of a TSR features two steel pipes in a telescopic arrangement, containing a porous filler. **Fehler! Verweisquelle konnte nicht gefunden werden.** shows the different components of the telescope element.
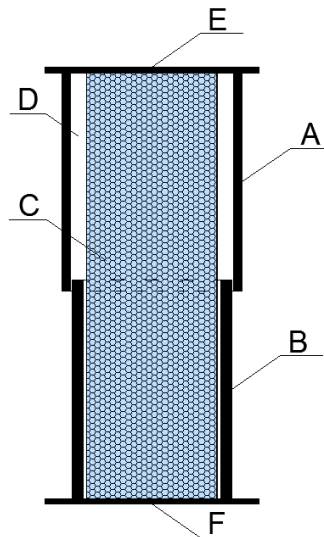
A	Outer pipe
B	Inner pipe
C_1	Porous filling
C_2	Other filling elements
D	Amount of free space
E	Head plate
F	Foot plate

Figure 2-4: Telescope element with legend.

2.1.2 Aim of the setup

At the beginning of the deformation, when the shotcrete has a low strength, the load should be transferred entirely through the filler. With increasing deformation and increasing shotcrete strength, the filler compacts, increasing its resistance. Due to the lateral expansion of the filler, the steel pipes buckle, thus contributing to the load transfer. The filler is squeezed into the buckling folds, thus preventing the otherwise inevitable drop in the systems resistance. A more or less constant increase in the load with displacement should follow.

3 Materials

This section describes some characteristics of the materials used for the laboratory tests.

3.1 Filling (C1)

At the beginning of the deformation process of the TSR, the porous cement bonded filling should carry the load only, in order not to overload the young shotcrete. On the one hand, to get a large deformation of the TSR (e.g. 5% for < 1000 kN), a high porosity of the filling material and/or free space between the filling and the steel pipes (D, see Figure 2-1) is necessary. On the other hand, it is necessary to ensure that the filling is not too porous, because the load capacity would decrease to an unacceptable low amount.

3.1.1 Filling material

For the production of the porous cement bonded filling, following materials, singularly or in combination, were tested:

- Portland cement (42,5 N/mm2 compressive strength after 28 days of curing time)
- Expanded clay by Liapor (Liapor, 2014).
    - Liapor, grain size 1-4 mm
    - Liapor, grain size 4-8 mm
    - Liapor, grain size 8-16 mm
- Sand, grain size < 2 mm
- Quartz sand, grain size 2 mm
- Cellular concrete by Ytong (Ytong, 2014).
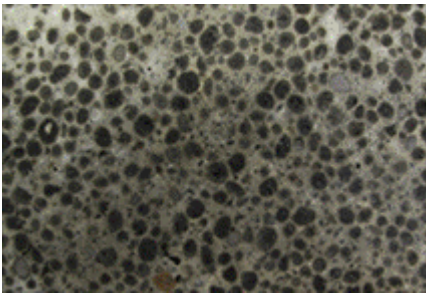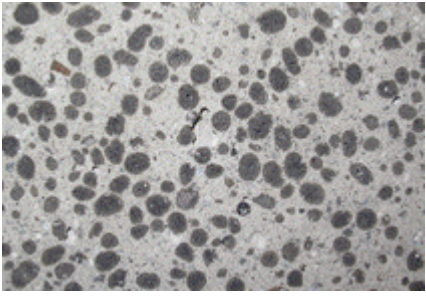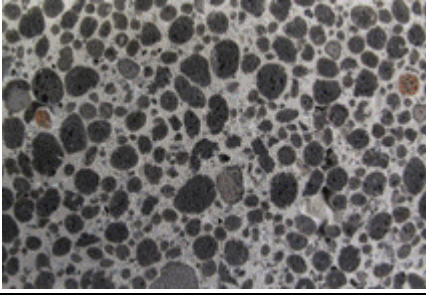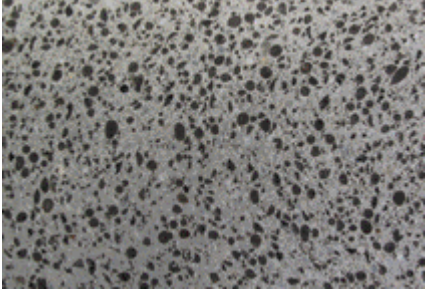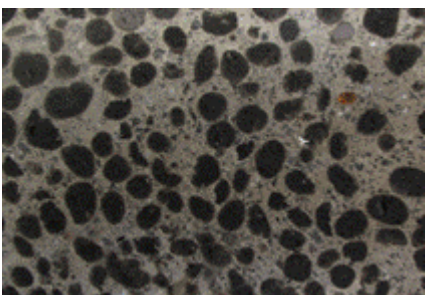
Various mixing ratios have been tested.

Because of the high water absorption of the Liapor a higher water/cement ratio is necessary, which can be evaluated with formula (1) by (Sitzwohl, 2011).

$$W/_C \, ratio = 0.4 + 0.15 * \frac{n_{Liapor}}{n_{cement}} \qquad (\, 1 \,)$$

To allow assessing the homogeneity and the distribution of the grains, some filling specimens were cut in half, which are shown in Table 3**.**

Table 3: Grain distribution of tested fillings.

	30%......Cement 50%.…..Liapor 4-8 20%.......Sand W/C-ratio = 0.45	Test number 1.6
	40%......Cement 40%......Liapor 4-8 20%......Sand W/C-ratio = 0.45	Test number 1.1
	20%......Cement 30%......Liapor 4-8 40%......Liapor 8-16 10%......Sand W/C-ratio = 0.75	Test number 1.2 1.3 1.4
	30%.…...Cement 40%.…...Liapor 1-4 30%.…...Sand W/C-ratio = 0.53	Test number 1.7
	20%......Cement 60%......Liapor 8-16 20%......Sand W/C-ratio = 0.85	Test number 1.5

3.1.2 Filling shape

Before the laboratory tests could start, a shape for the filling had to be found. The filling should be easy to produce, and should provide an additional amount of free space between the filling and the steel pipes to allow even more deformation, as Sitzwohl (2011) already stated in his thesis.

3.1.2.1 Hexagonal shape

After some considerations, a hexagonal shape was chosen (Figure 3-1). The advantage of this shape lies in the easy manufacturing process. A high number of fillings can be produced easily in a short period.
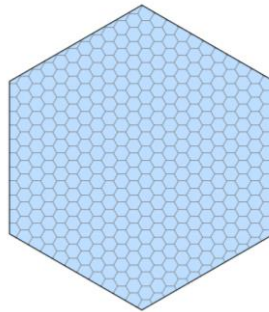
Figure 3-1: Hexagonal shape of the porous cement bonded filling.

For the shuttering of the hexagonal shape, trapezoidal metal sheets have been used. The trapezoidal metal sheets were custom manufactured to obtain the ideal shape and size for the fillings. The result of putting together two mirrored trapezoidal sheet metals, is a hexagonal form. The production of such a shuttering is quite easy and it can be used multiple times. In order to increase the stability wooden boards were used as casing.

Figure 3-2: Shuttering for hexagonal shaped fillings.

3.1.2.2   Circular shape (lost formwork)

Another considered shape was the circular shape including a 0.6 mm steel cover. These specimens worked quite well because the steel cover prevented the shearing-off effect of the filling (Figure 3-3).

Figure 3-3: Circular shape of the porous cement bonded filling with steel cover.

The sheet iron pipe was used as lost formwork (Figure 3-4). This type of filling is not as easy to produce and it is more expensive due to the lost formwork. However, the stability in the test procedure is better than that of the hexagonal shape.
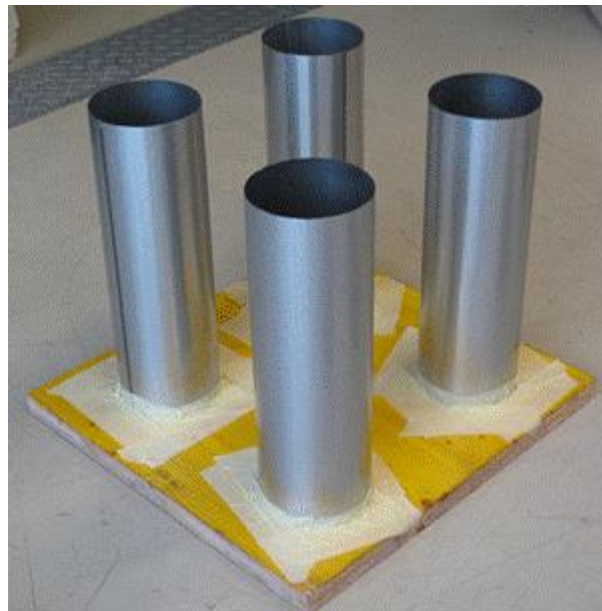
Figure 3-4: The circular shuttering (lost formwork).

3.2 Elastic / Plastic inlays (C2)

In the fifth test series different elastic or plastic inlays were tested. The purpose was to postpone the failure of the filling and obtain a smoother load development. Four different materials with different behaviours were tested. Two of them were made of rubber (Figure 3-5), one was a polyurethane plate (Figure 3-6) and the last plate was made of cork (Figure 3-7). All these plates were installed in the elements with a height of 2 cm.

Figure 3-5: Rubber plates (red: soft; black: medium).

Figure 3-6: Polyurethane plate with aluminium cover.

Figure 3-7: Cork plate.

3.3 Steel pipes (A, B)

3.3.1 First test series

The steel pipes in the first test series were very solid and consisted of S355 steel (construction steel with a yield strength of 355 N/mm^2). The inner pipe (B) had an inner diameter of 126 mm and a wall thickness of 10 mm. The outer pipe (A) had an inner diameter of 149.1 mm and a wall thickness of 8 mm. All these elements had the same height of 400 mm.

3.3.2 Second test series

This series includes just one test. Two steel iron pipes (A, B) with a wall thickness of 0.6 mm were tested. The purpose was to assess the properties of the filling without a big influence of the steel pipes.

3.3.3 Third test series

Stovepipes were used in the third test series. The quality of these pipes was S235 steel (construction steel with a yield strength of 235 N/mm^2). The pipes had a wall thickness of 2 mm. The inner pipe (B) had an inner diameter of 120 mm and the outer pipe (A) had an inner diameter of 130 mm. With this set-up, a shortening of 73% was possible.

3.3.4 Fourth test series

In this series, stovepipes were used with the same quality and the same wall thickness as for the third test series. The inner and outer diameters of the pipes were 130 mm and 150 mm.

3.3.5 Fifth test series

For these tests, different elastic or plastic inlays (C2) were tested. The filling and the steel pipes were the same as for the fourth test series. The purpose was to provide an additional soft cushion, delaying the load development.

4 Lab tests

The tests were executed in the laboratory of the Institute for Rock Mechanics and Tunnelling on the compression test apparatus.

4.1 Test procedure

The procedure was the same for all tests. The load rate of the tests was 2 mm/min. The force and the axial displacement were measured. The maximal stroke of the machine is 10 cm. After 10 cm of compression, additional rings are inserted and the test continued (see Figure 4-1).

Two termination criteria for the test were:

- After 10 cm displacement the machine stops and the measured data is saved.
- The force exceeds the limit of approximately 2700 kN (capacity of the hydraulic loading system).

A few tests we aborted manually. Either because the maximal deformation was reached before the force limit, or because the set-up of the yielding element led to undesirable results. Chapter 4.2 only includes results and interpretations of tests not aborted manually.
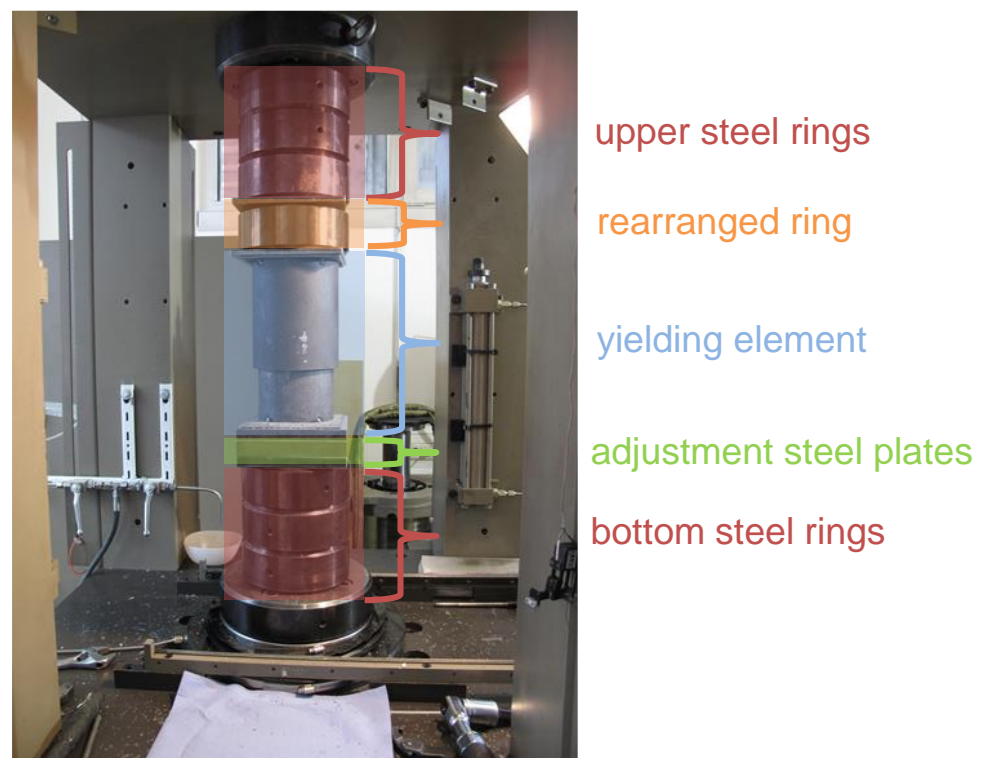
Figure 4-1: Triaxial compression test apparatus.

4.2 **Test results**

Different types and combinations were tested in the laboratory.

4.2.1   First test series

In this test series massive steel pipes were used, including a hexagonal shape of a porous cement bonded filling. Different mixtures for the filling were tested.

In the first test (test number (1.1)), the upper pipe had the bigger diameter. Figure 4-1shows the test results. After reaching the uniaxial compressive strength (UCS) of the filling material, a load drop occurs. For the next 20% shortening of the element the load increased very slowly, because of the porosity of the filling and the additional free space within the steel pipes. When the majority of the pores had collapsed and the free space was nearly filled, the force increased rapidly.
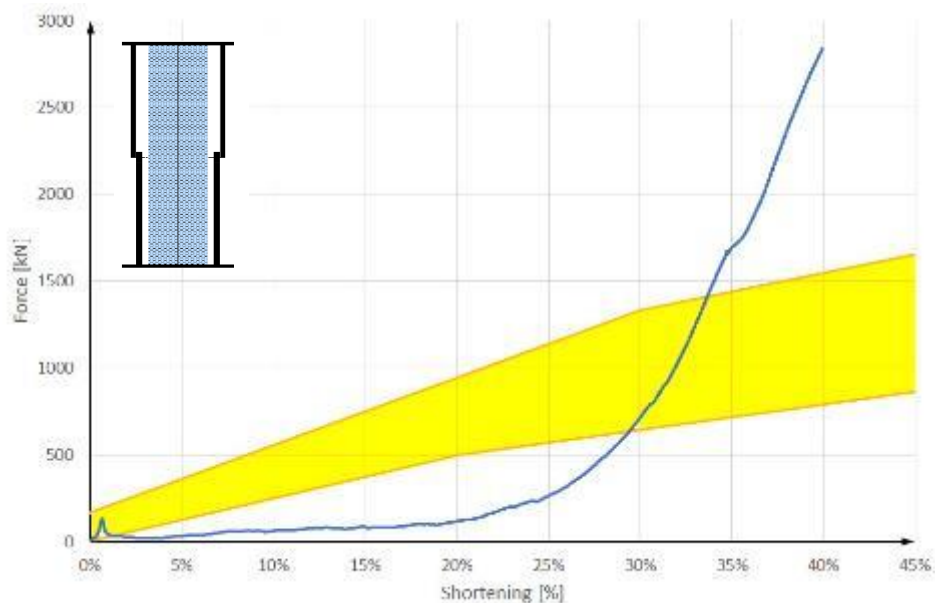
Figure 4-2: Force-shortening diagram of test number (1.1).

Because of the load drop and the flat load development, the element set-up of this test is not suitable. To avoid the load drop, the sudden shear failure of the filling had to be prevented.

The next elements were installed upside down, so that the bottom pipe had the bigger diameter. For test number (1.3), the additional free space in the bottom pipe was filled with fine sand in order to eliminate the extreme load drop (Figure 4-3). The sand filling accomplished its task, but the elements got too heavy and the production process became more complex.

For test number (1.4.1), (1.4.2) and (1.5) the set-up was the same, but instead of sand,

"Liapor 1-4" was used. Liapor is a product name for expanded clay and 1-4 describes the grain size mixture in mm (Figure 4-4).
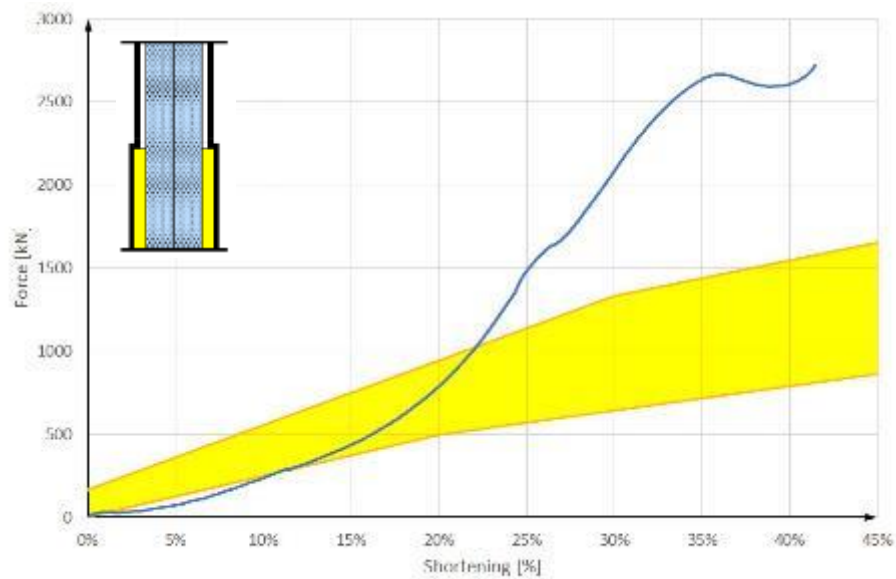
Figure 4-3: Force-shortening diagram of test number (1.3).

▬	Test number 1.4.1
▬	Test number 1.4.2
▬	Test number 1.5
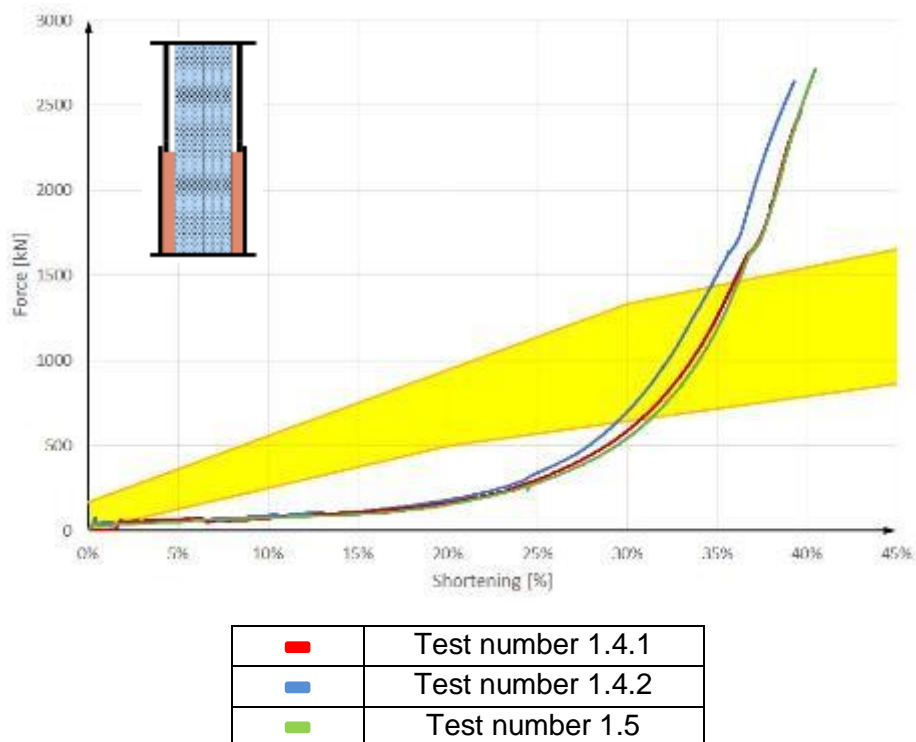
Figure 4-4: Force-shortening diagram of test number (1.4 - 1.5).

The peak at the beginning could almost be eliminated, but the load within the first 20% of shortening develops too slowly and too rapid afterwards.

The next step was to find a filling that allows a continuous force increase. Different combinations and mixtures for the filling were produced and tested. One idea was to use

two fillings with different properties in the element, one at the top and one at the bottom of the element.

Figure 4-5 shows two curves, each of them with two different fillings and without a filling in the free space.

▬ (red)	Test number 1.6
▬ (blue)	Test number 1.7
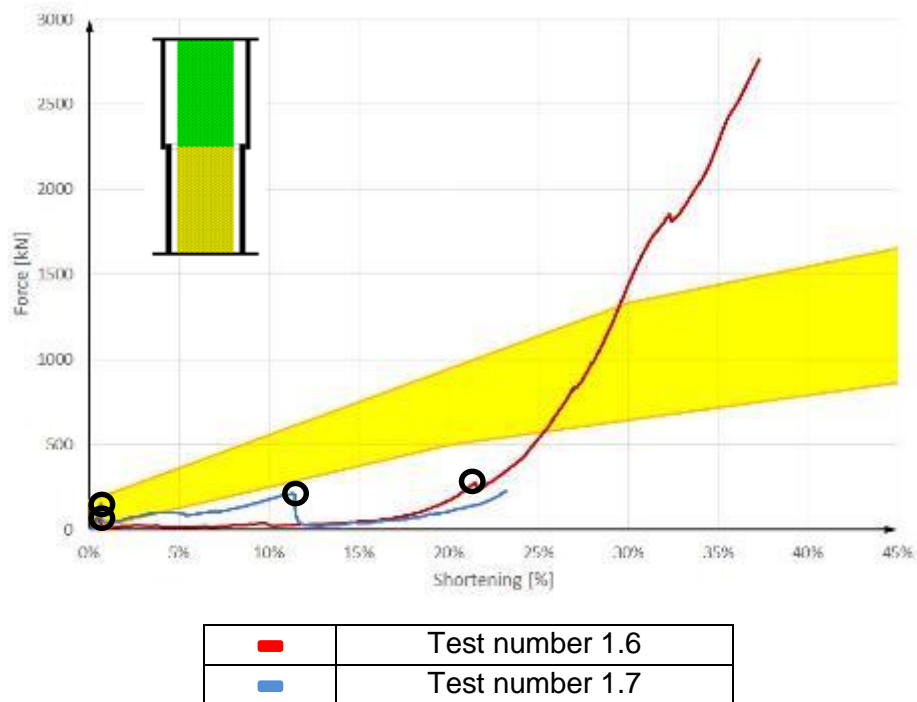
Figure 4-5: Force-shortening diagram of test number (1.6; 1.7).

In both curves, two main peaks occur at the beginning (black circles at ~0.5% of shortening). At this load level, the filling reaches the uniaxial compressive strength (UCS), resulting in a loss in resistance. The yielding element (1.6) (red curve) shows roughly the same behaviour as the elements tested before. The force increment is still too low after the load drop. The only difference is a higher oscillation due to the discontinuous failure of the two fillings. This behaviour is even more pronounced for the yielding element (1.7) (blue curve).

In the next test, a simple Ytong block was used as the filling (test number (1.8)). It turned out that this material cannot resist the high forces, so no further tests with Ytong were conducted.

To counteract the effect of the load drop a steel pipe with a diameter of 25 mm and a wall thickness of 0.6 mm was inserted centrically in the hexagonal filling of the element (test number (1.9)). This additional pipe should support the filling and prevent the high load drop at the beginning (Figure 4-6).

Figure 4-6: Additional centrically arranged steel pipe.
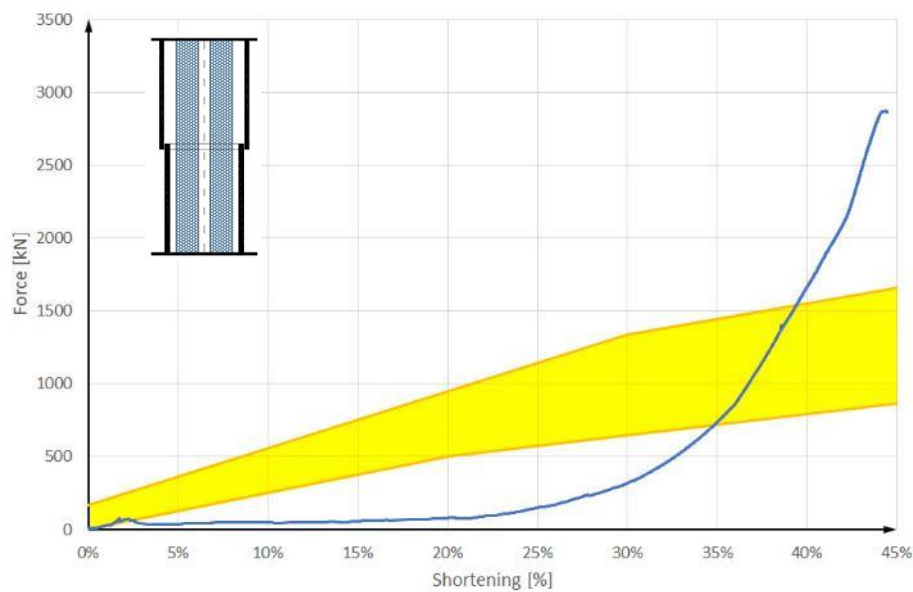
Figure 4-7: Force-shortening diagram of test number (1.9).

As one can see in Figure 4-7, the steel pipe has almost no influence on the force-shortening behaviour. The problem is the buckling of the central pipe. When the pipe buckles, the filling is destroyed and can´t mobilize any counteracting force. Therefore, this type of filling does not yield the intended effect.

The main problem of the previous tests was the shearing of the fillings In further test series a steel iron pipe with a wall thickness of 0.6 mm as lost formwork was used. This steel cover around the filling prevents shearing and decomposition of the filler. Figure 4-8 shows the result of the test.
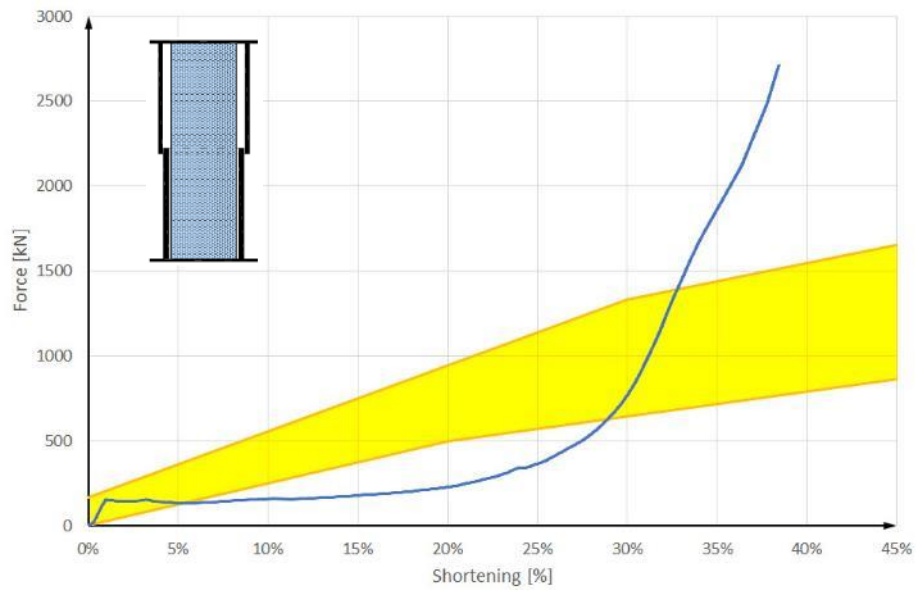
Figure 4-8: Force-shortening diagram of test number (1.10).

Figure 4-9: Bottom steel pipe and filling with lost formwork of test number (1.10).

4.2.1 Second test series

In order to examine the pore volume after the compression, the element was cut in half (Figure 4-10). It became obvious, that the main problem of the element is the massive wall thickness. The main load transfer occurs at the contact area of the inner pipe. After some deformation, the steel element carries the entire load and the filling plays a minor role. Another problem was that these thick pipes do not buckle, so the granular structure does not change during the deformation process and big deformations are not possible. The next logical step was to use pipes with a thinner wall thickness to allow larger deformation.
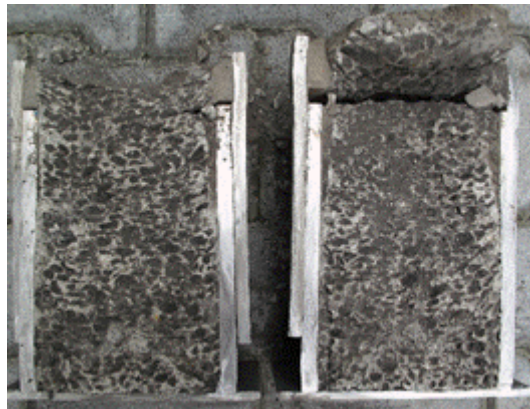
Figure 4-10: (test number (1.5)) cut in half.

In this test series the aim was to determine the behaviour of the filling without a big influence by the steel pipes. A steel iron pipe with a wall thickness of 0.6 mm was used as element instead of the massive steel pipes with a wall thickness of almost 10 mm. At this stage of the thesis, it was stated that the hexagonal shape and the massive pipes are not the right choice for the telescope-yielding-element. The results of this series (test number (2.1)) are shown in the Appendix A (see page 30).

4.2.2   Third test series

In this test series stovepipes with a wall thickness of 2 mm were used. For the tests, pipes with 120 mm, 130 mm and 150 mm diameter were used.

To investigate the differences between the massive and the thin-walled elements we used the same fillings for this test series as for test number (1.1), (1.9) and (1.10). The Figures 4-11 to 4-13 depict the results of the test series.

These tests clearly illustrate that the pipes with the thinner wall thickness can absorb almost double the deformation compared to the pipes with the massive wall thickness, due to the buckling of the thinner steel pipes. With this type of element more than 60% of shortening is possible, observable for all tests. The load development is very similar to the results of the previous test with the thick walled pipes on the first 20% of shortening, indicating that the load is only transferred via the filler.

▬	Test number (1.1) with the massive pipes
▬	Test number (3.1) with the stovepipes
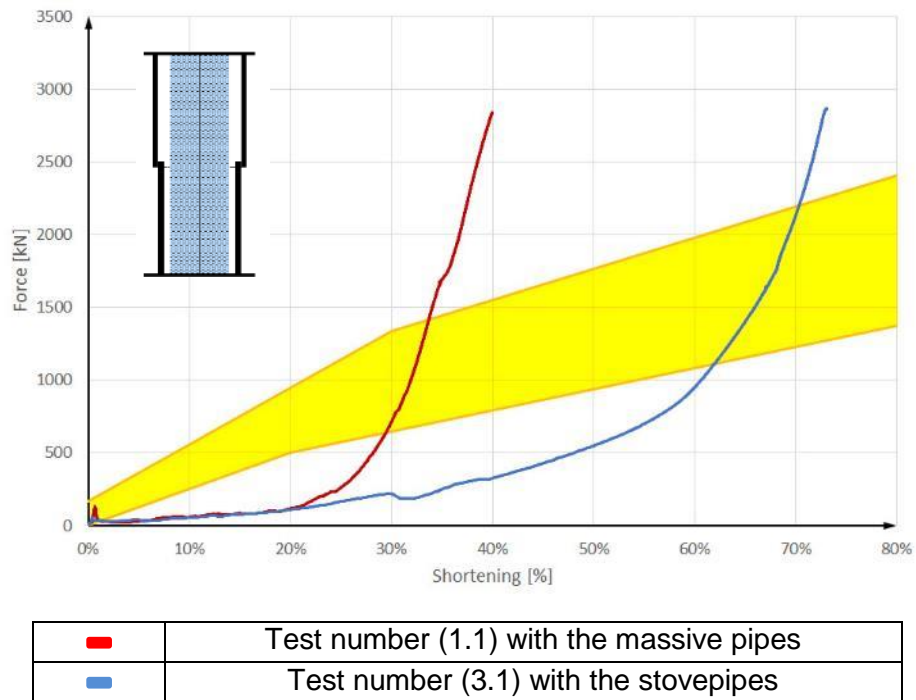
Figure 4-11: Force-shortening diagram of test number (3.1); comparison with test number (1.1).

Figure 4-12 shows the test with a hexagonal filling and an additional steel pipe in the centre. The diagram shows that the first 30% for both, the massive and thin-walled element are almost the same, but afterwards the stovepipes allow larger deformations.

▬	Test number (1.9) with the massive pipes
▬	Test number (3.2) with the stovepipes
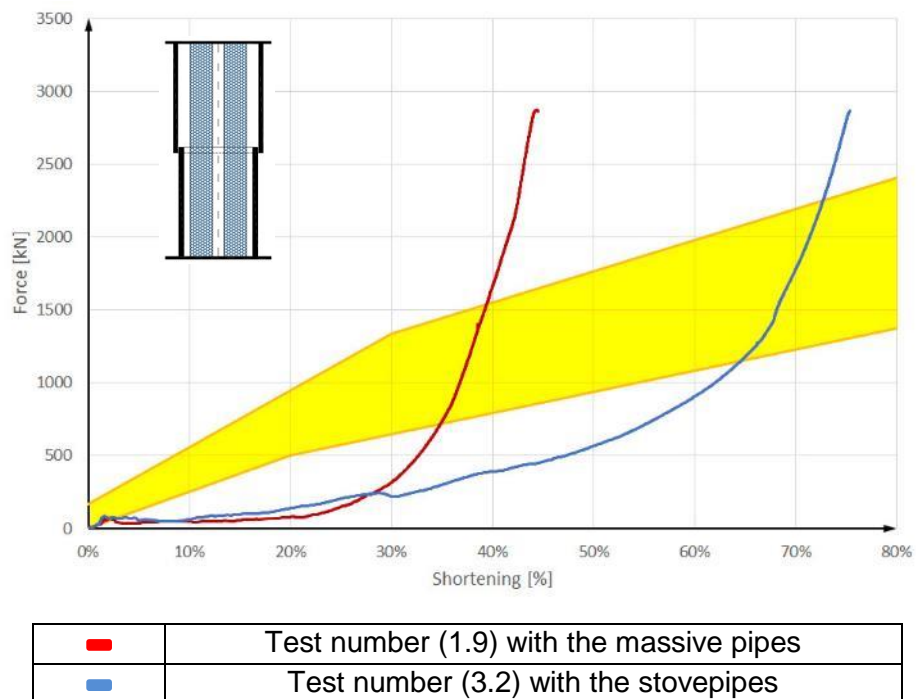
Figure 4-12: Force-shortening diagram of test number (3.2); comparison with test number (1.9).

The same characteristic is shown in Figure 4-13 for test number (3.3). For this element the filling with a lost formwork of steel was used to minimise shearing. This type of filling has the ideal properties to achieve the required force-shortening behaviour. Due to the stabilisation of the filling by the lost formwork, no load drop is observed. Hence, for all following tests the same type of filling was used.
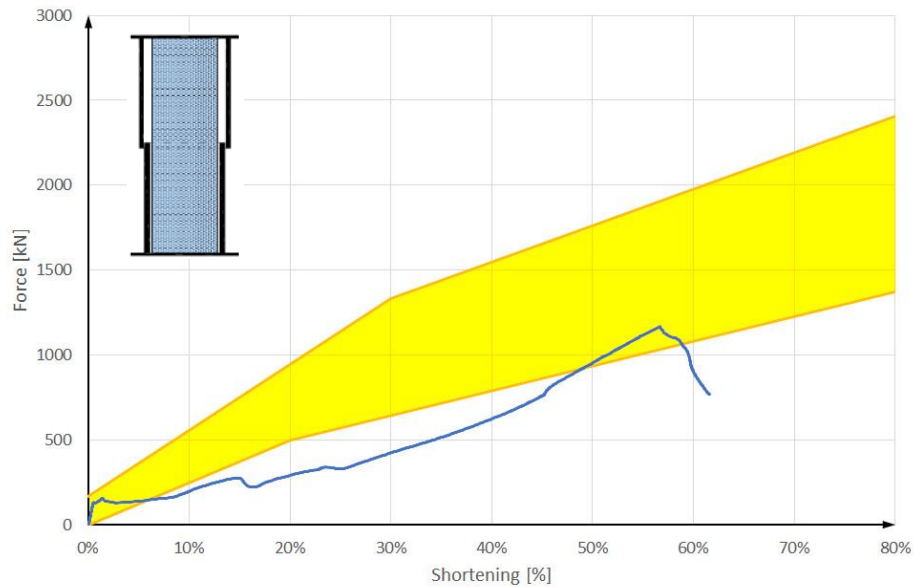
Figure 4-13: Force-shortening diagram of test number (3.3).

Figure 4-14: Stovepipe element with crack.

Bursting of the steel element (Figure 4-14) caused a load drop at the end of the test (Figure 4-13).

The specimen with the steel cover around the filling worked quite well in the load tests. This type of filling solves the problem of the load drop at the beginning.

4.2.3 Fourth test series

In the fourth series of lab tests, different combinations of steel pipe lengths were tested. The idea was to mobilize more resistance after a certain amount of deformation, leading to a higher increase of the force.

Figure 4-15 shows the two combinations tested. For sample 9, the filling was 2 cm longer than the inner bottom pipe. For sample 10, the filling was of the same length as the inner bottom pipe. For both elements, steel pipes cover the fillings.

The goal of using different heights was to control at which point of deformation more resistance mobilizes.

Figure 4-15: Yielding elements (test number (4.1) and (4.2)) of the fourth test series.

	Sample 9 (Test number (4.1))
▬	(filling 2 cm longer than the inner pipe)
▬	Sample 10 (Test number (4.2))
	(filling and inner pipe of the same length)
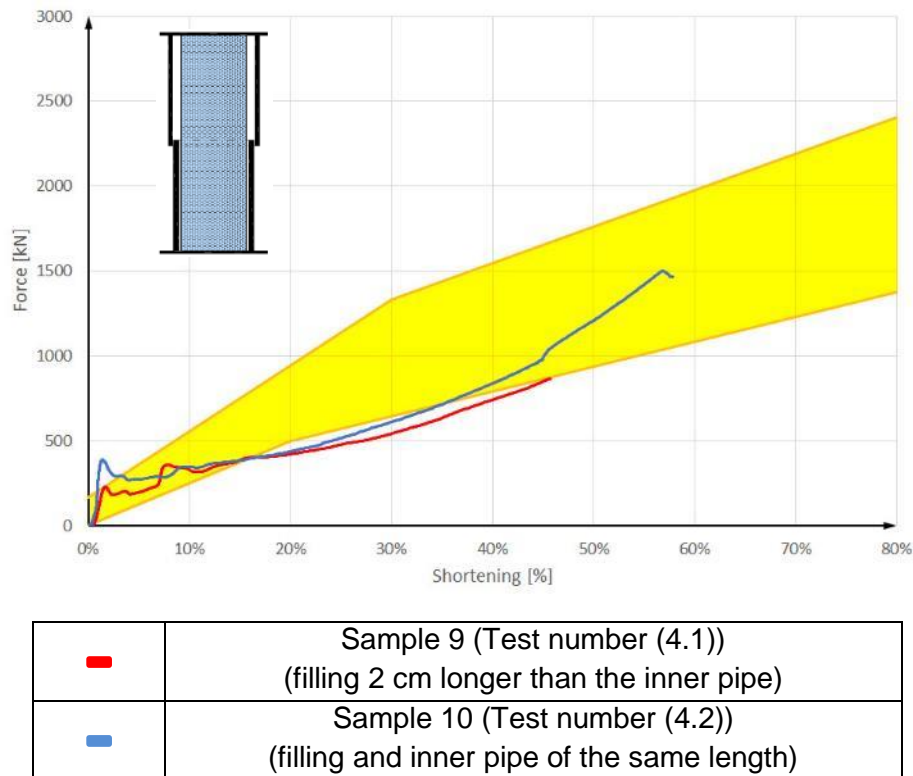
Figure 4-16: Force-shortening diagram of test number (4.1; 4.2); different length of the inner pipe.

Sample 10 shows the first peak between 350 kN and 400 kN and after 8% or 2 cm of shortening, respectively. Sample 9 has a peak between 350 kN and 400 kN as well (Figure 4-16). Therefore, with minor modifications it is possible to delay this peak to a certain amount of shortening.

4.2.4 Fifth test series

In the fifth test series four different inlays with a height of 2 cm and with different properties were tested (shown in Figure 4-17). These inlays should postpone the point of the first peak, which means a slightly flatter trend at the beginning of the force-shortening-curve. This also results in more time for the hardening of the shotcrete at site. The mixture of the filling was for all four samples was the same.
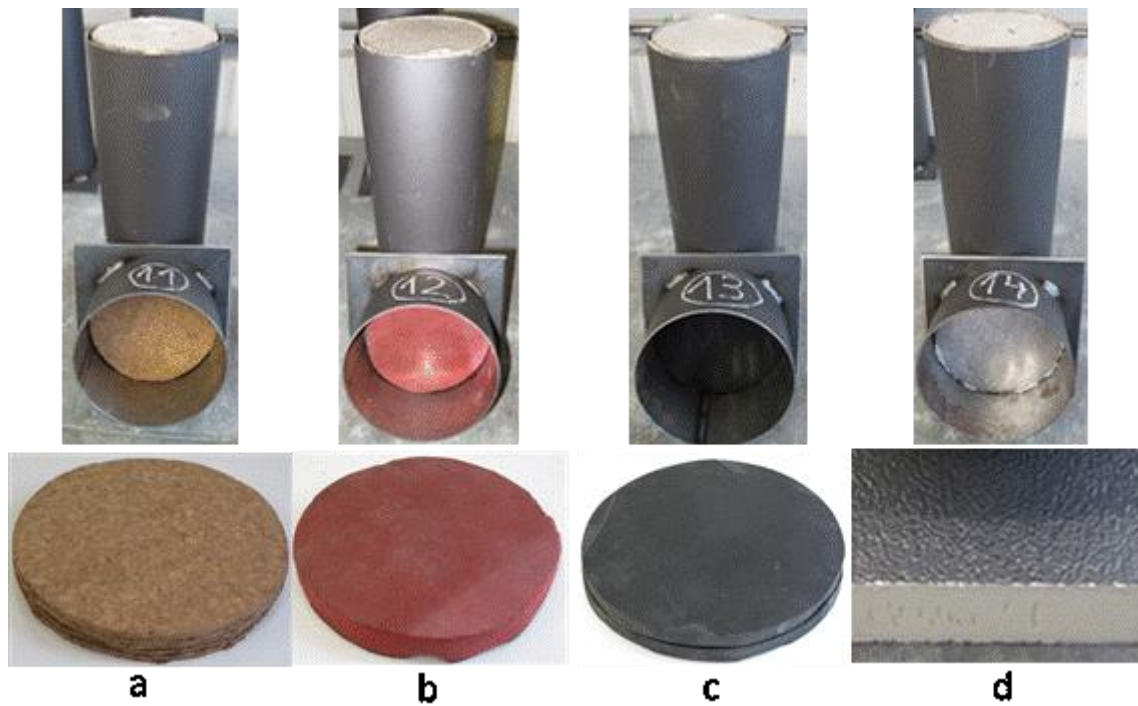
Figure 4-17: a) Cork; b) soft rubber; c) medium hard rubber; d) polyurethane with aluminium cover.

With these inlays it could be prevented that the first peak of the curve is outside the ideal-characteristic-area. This implies that the shotcrete will not be damaged.

Figure 4-18 shows a comparison of the last five tests for the first 45% of shortening.

The black curve represents the result of test number (4.2), having the same filling but without an inlay.

The first major peak occurs for all five elements at roughly 400 kN. In contrast to the element without an inlay (black curve), for the elements with an inlay the peak occurs at a later point of shortening.
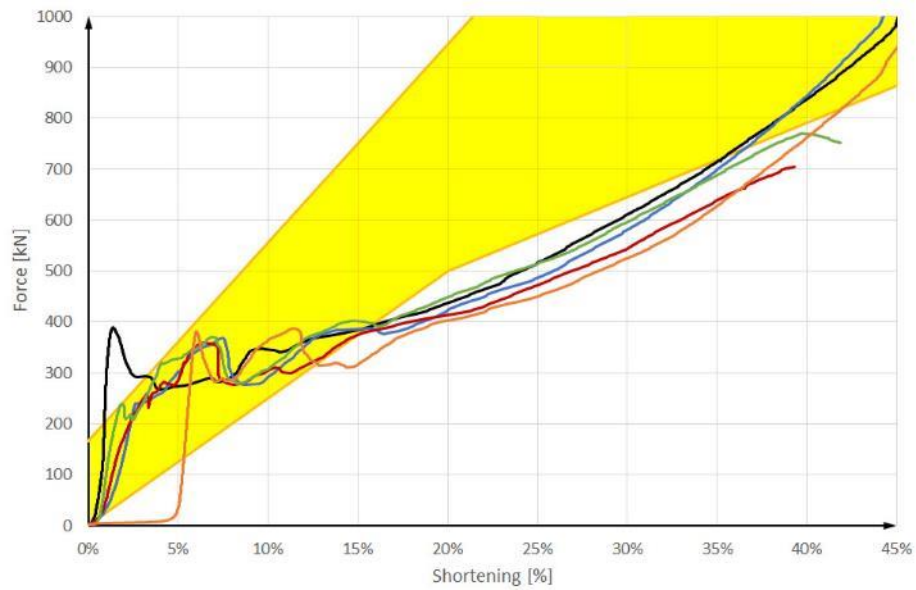
	Sample 10 (Test number (4.2)) (filling and inner pipe of the same length)
■ (blue)	Cork inlay
■ (red)	Soft rubber inlay
■ (green)	Medium hard rubber inlay
■ (orange)	Polyurethane inlay

Figure 4-18: Force-shortening diagram of test number (4.2; 5.1; 5.2; 5.3; 5.4).

In the last six tests (4.1 – 5.4) the load between 15% and 40% of shortening is below the target range. Increasing the wall thickness of the pipes, or slightly modifying the filler should solve this problem.

5 Conclusion

After some try and error in the beginning of the work, a combination of steel pipes and filler could be found, which is close to fulfilling the defined requirements. Relatively thin walled steel pipes were found to be suitable as confinement for the filler. The filler itself contains a mix of cement, expanded clay bubbles, and sand. The filler itself is cast into a lost formwork of a steel pipe with a wall thickness of 0,6 mm, preventing premature decomposition of the filler, while still allowing space for lateral expansion during the deformation process.

Adjustment to the initial response of the elements to loading was achieved by using inserts of various materials.

Additional fine tuning is required in order to reduce the elements response in the early phase of deformation, and to increase the load development in the range between 15% and 30% of shortening. This can be obtained by using different insert materials, modifying the properties of the filler and the pipe wall thicknesses.

References

Feder, G., & Arwanitakis, M. (1976). Zur Gebirgsmechanik ausbruchsnaher Bereiche tiefliegender Hohlraumbauten. *Berg- und Hüttenmännische Monatshefte, 121*(4), pp. 103-117.

Liapor. (2014). Retrieved from http://www.liapor.com/en/start.php

MathWorks (2004): *MatLab. Electronic User Manual, Non-linear optimisation toolbox MathWorks, Natick, 2004.*

Pacher, F. (2010). Gebirgs- und Ausbaukennlinien. *Geomechanics and Tunnelling, 4*(3), pp. 402-408.

Panet, M., & Guenot, A. (1982). Analysis of convergence behind the face of a tunnel. *Tunneling 182*, 197-204.

Radončić, N. (2011). Tunnel design and prediction of system behavior in weak ground. Doctoral Thesis, Institute for Rock Mechanics and Tunnelling.

Radončić, N., Pilgerstorfer, T., & Schubert, W. (2008). *Prediction of displacements in tunnels.* ISRM International Symposium - 5th Asian Rock Mechanics Symposium, 24-26 November, Tehran, Iran; 809-819.

Radončić, N., Schubert, W., & Moritz, B. (2009). Ductile support design. *Geomechanics and Tunnelling 2*(5), pp. pp. 561-575.

Schubert, P. (1988). Beitrag zum rheologischen Verhalten von Spritzbeton. *Felsbau 6, 3*, pp. 150-153.

Sitzwohl, M. (2011). *Optimierung der Lining Stress Controller durch zementgebundene poröse Füllung.* GrazGraz University of Technology, Austria: Master Thesis, Institute for Rock Mechanics and Tunnelling.

Sulem, J., Panet, M., & Guenot, A. (1987). Closure analysis in deep tunnels. *Int. Journal of Rock Mechanics and Mining Science, 24*.

Ytong. (2014). Retrieved from http://www.ytong.at

Appendix A

Steel parts of the Yielding Elements

Steel quality: S355; S235

Specific weight of the materials

Material	Specific weight ρ_D [g/cm³]
Cement CEM II/A-M (S-L) 42,5 N WT 38	1.07
Liapor 1-4 mm	0.44
Liapor 4-8 mm	0.37
Liapor 8-16 mm	0.35
Sand < 2 mm	1.56
Water	1.00

Dimensions

	outer diameter [mm]	inner diameter [mm]	wall thickness [mm]	height [mm]
outer pipe	165.1	149.1	8.0	200
inner pipe	146.0	126.0	10.0	200
total				390

Sketch
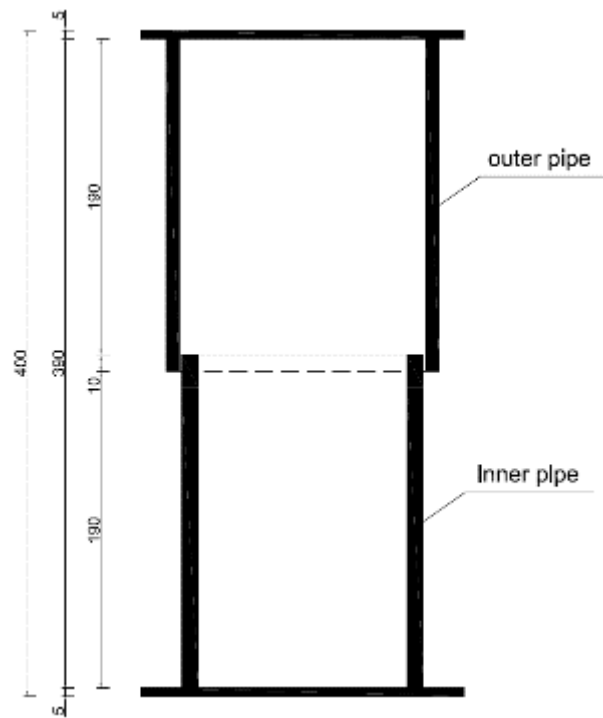
Picture

Yielding element (first test series)

Test number: 1.1
Lab number: 40/40/20
Height: 400 mm
Type: TSR
Outer diameter: 165.1 mm
Comment: The first test with a hexagonal filling.

Mixture of filling

	Volumetric content	Volumetric percent	Weight content
Cement	1	40	1
Liapor 4-8 mm	1	40	0.35
Sand < 2 mm	0.50	20	0.73
Water	-	-	0.45

Picture

Characteristic curve

Yielding element (first test series)

Test number: 1.2
Lab number: 20/30/40/10
Height: 400 mm
Type: TSR
Outer diameter: 165.1 mm
Comment: This test was aborted after the first 10 cm of shortening, because of the high load drop.

Mixture of filling

	Volumetric content	Volumetric percent	Weight content
Cement	1	20	1
Liapor 4-8 mm	1.5	30	0.52
Liapor 8-16 mm	2	40	0.65
Sand < 2 mm	0.5	10	0.73
Water	-	-	0.75

Picture

Characteristic curve
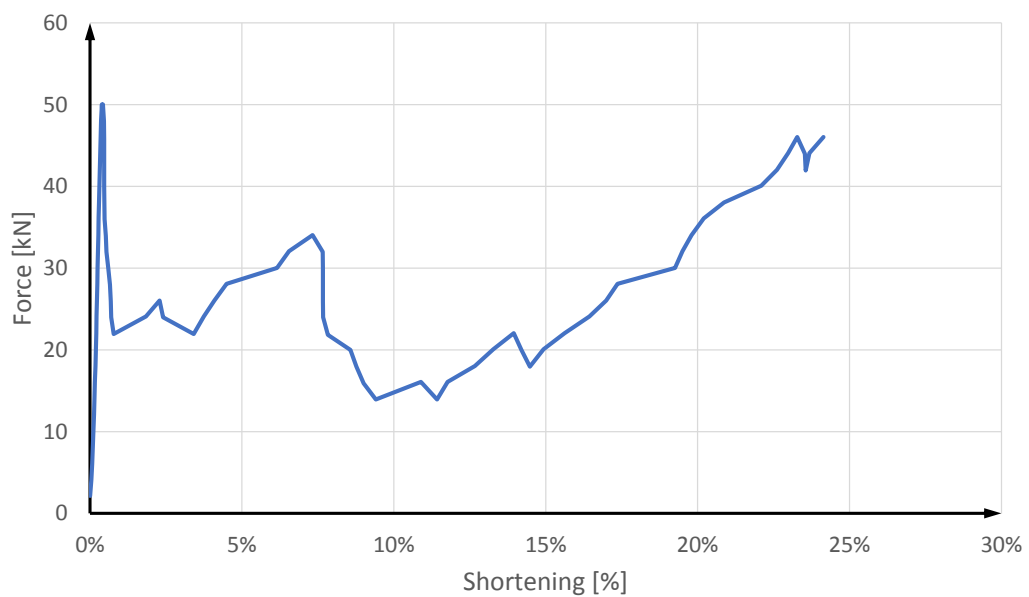
Yielding element (first test series)

Test number: 1.3
Lab number: 20/30/40/10 + sand
Height: 400 mm
Type: TSR
Outer diameter: 165.1 mm
Comment: Against the high load drop, the free space of the bottom pipe was filled with sand.

Mixture of filling

	Volumetric content	Volumetric percent	Weight content
Cement	1	20	1
Liapor 4-8 mm	1.5	30	0.52
Liapor 8-16 mm	2	40	0.65
Sand < 2 mm	0.5	10	0.73
Water	-	-	0.75

Picture

Characteristic curve
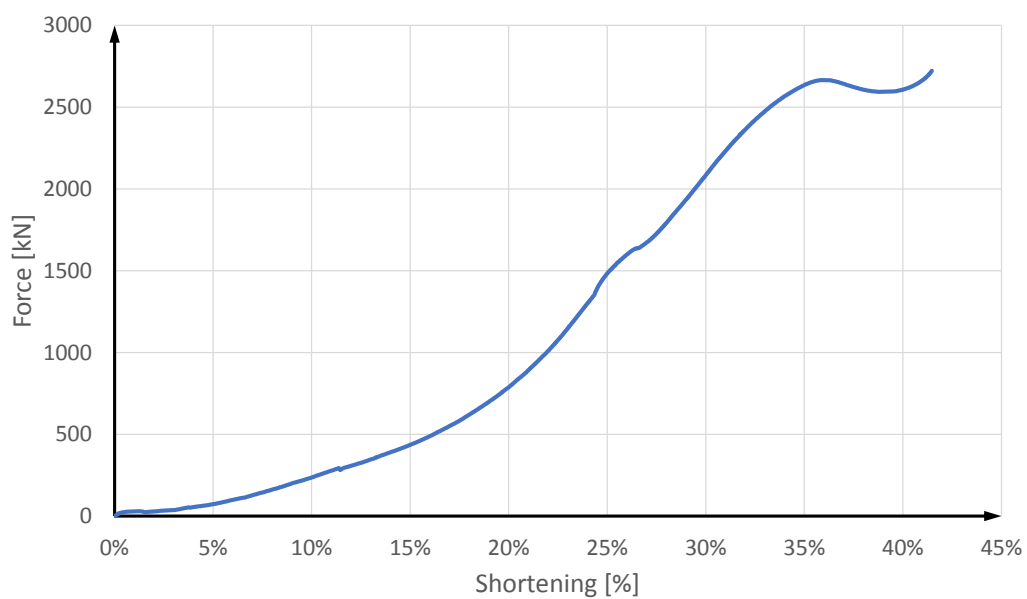
Yielding element (first test series)

Test number: 1.4.1
Lab number: 30/25/35/10 + Liapor 1-4
Height: 400 mm
Type: TSR
Outer diameter: 165.1 mm
Comment: Against the high load drop, the free space of the bottom pipe was filled with Liapor.

Mixture of filling

	Volumetric content	Volumetric percent	Weight content
Cement	1	30	1
Liapor 4-8 mm	0.83	25	0.29
Liapor 8-16 mm	1.17	35	0.38
Sand < 2 mm	0.33	10	0.49
Water	-	-	0.60

Picture

Characteristic curve
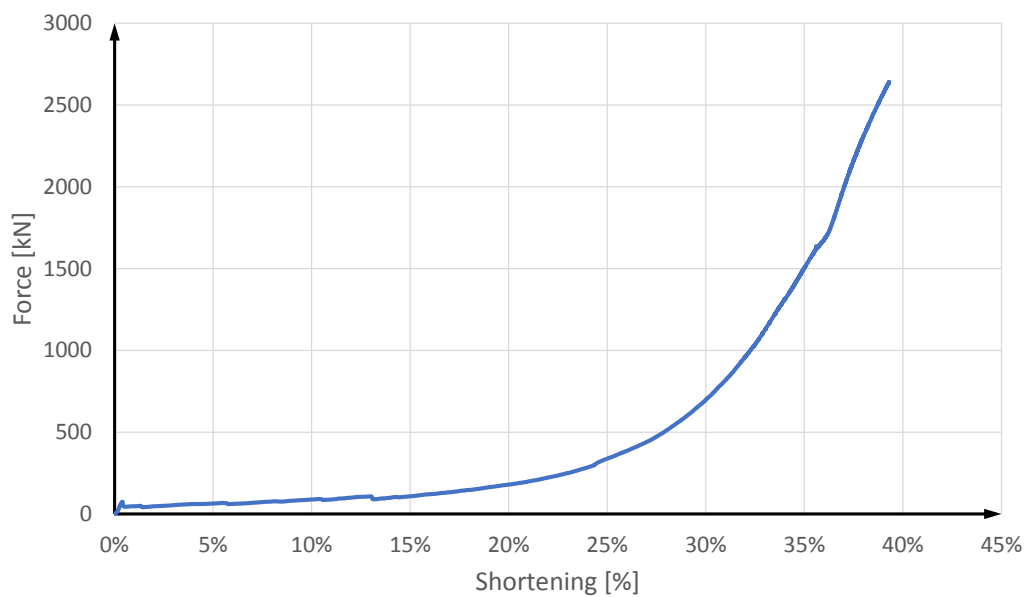
Yielding element (first test series)

Test number: 1.4.2
Lab number: 30/25/35/10 + Liapor 1-4 2nd
Height: 400 mm
Type: TSR
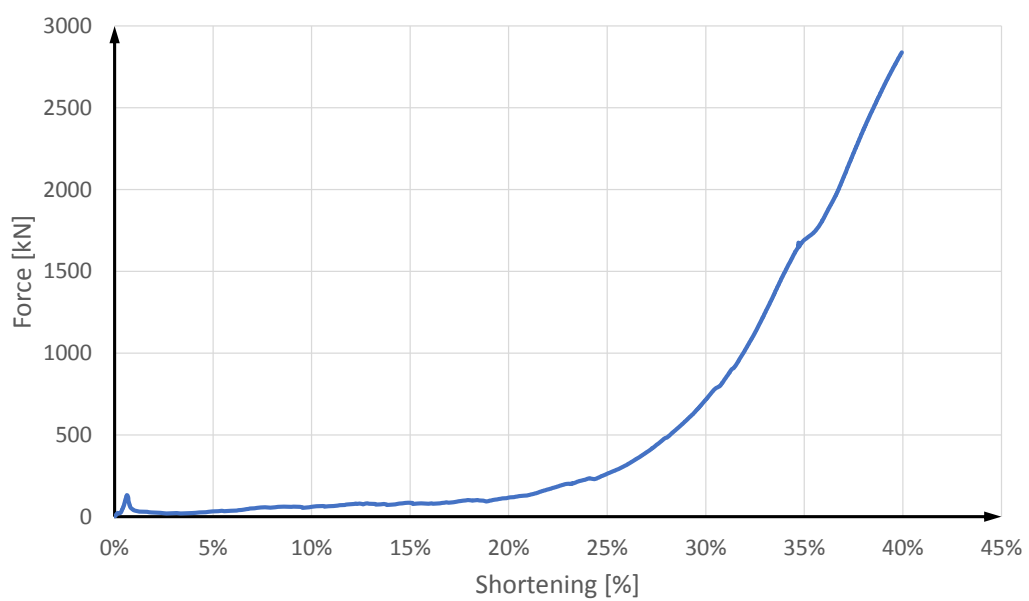Outer diameter: 165.1 mm
Comment: This test is the same as the test before, to determinate the deviation between two similar
                          tests.

Mixture of filling

	Volumetric content	Volumetric percent	Weight content
Cement	1	30	1
Liapor 4-8 mm	0.83	25	0.29
Liapor 8-16 mm	1.17	35	0.38
Sand < 2 mm	0.33	10	0.49
Water	-	-	0.60

Picture

Characteristic curve
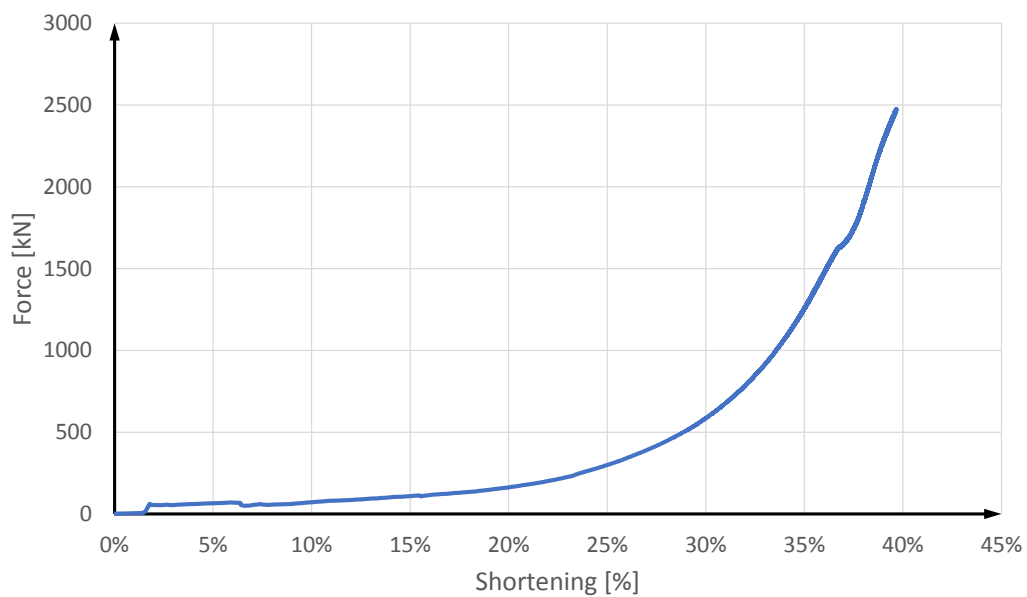
Yielding element (first test series)

Test number: 1.5
Lab number: 20/60/20 + Liapor 1-4
Height: 400 mm
Type: TSR
Outer diameter: 165.1 mm
Comment: After the test the element has been cut in the middle, to take a closer look at the pore
                       volume.

Mixture of filling

	Volumetric content	Volumetric percent	Weight content
Cement	1	20	1
Liapor 8-16 mm	3	60	0.98
Sand < 2 mm	1	20	1.46
Water	-	-	0.70

Picture

Characteristic curve
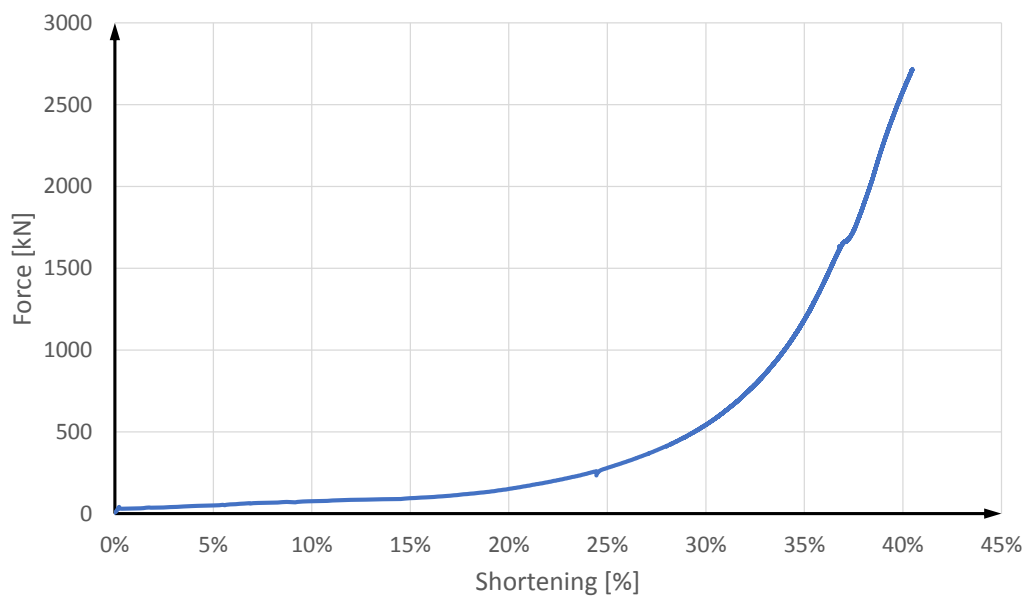
Yielding element (first test series)

Test number: 1.6
Lab number: 1
Height: 400 mm
Type: TSR
Outer diameter: 165.1 mm
Comment: Two different fillings in one element was tested.

Mixture of filling

upper part

	Volumetric content	Volumetric percent	Weight content
Cement	1	20	1
Sand < 2 mm	4	80	5.83
Water	-	-	0.40

lower part:

	Volumetric content	Volumetric percent	Weight content
Cement	1	30	1
Liapor 4-8 mm	1.67	50	0.58
Sand < 2 mm	0.67	20	0.97
Water	-	-	0.45

Picture

Characteristic curve
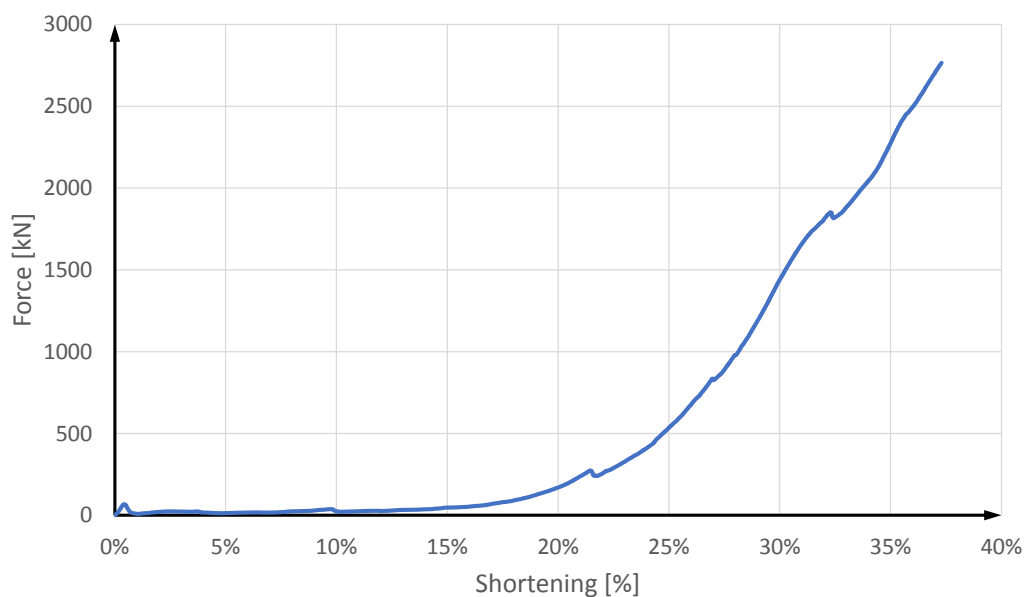
Yielding element (first test series)

Test number: 1.7
Lab number: 2
Height: 400 mm
Type: TSR
Outer diameter: 165.1 mm
Comment: Two different fillings in one element was tested. One can clearly identify the two UCS of the fillings.

Mixture of filling

upper part

	Volumetric content	Volumetric percent	Weight content
Cement	1	30	1
Sand < 2 mm	2.33	70	3.40
Water	-	-	0.40

lower part:

	Volumetric content	Volumetric percent	Weight content
Cement	1	30	1
Liapor 4-8 mm	1.33	40	0.55
Sand < 2 mm	1	30	1.46
Water	-	-	0.53

Picture

Characteristic curve
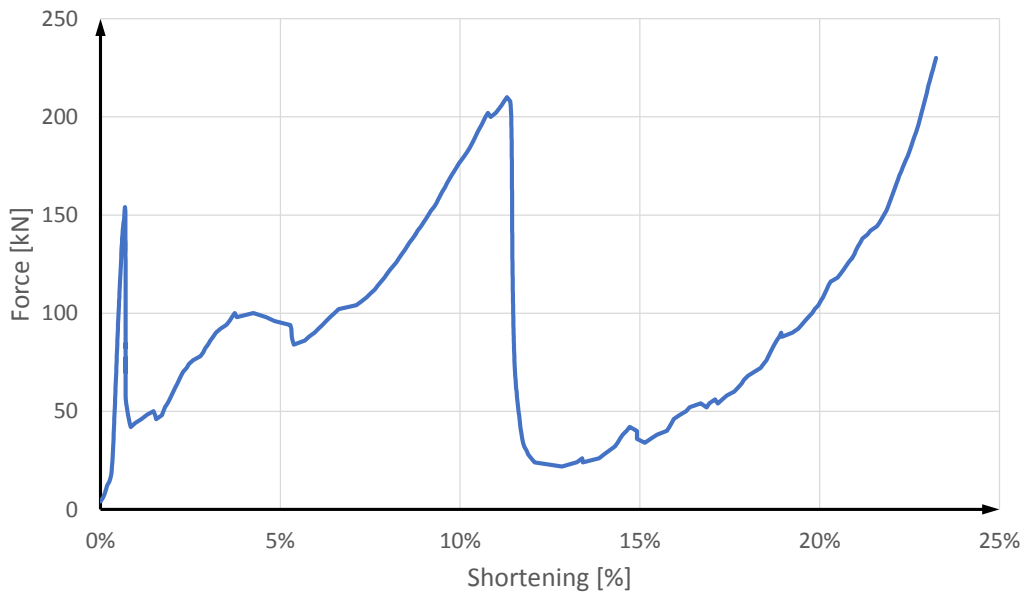
Yielding element (first test series)

Test number: 1.8
Lab number: 3
Height: 400 mm
Type: TSR
Outer diameter: 165.1 mm
Comment: A 9x9 cm Ytong block was the filling.

Mixture of filling

	Volumetric content	Volumetric percent	Weight content
Ytong	1	100	1

Picture

Characteristic curve

Yielding element (first test series)

Test number: 1.9
Lab number: 4
Height: 400 mm
Type: TSR
Outer diameter: 165.1 mm
Comment: A filling with a centrically arranged steel pipe
                      (diameter: 25 mm, wall thickness: 0.6 mm) was used.

Mixture of filling

	Volumetric content	Volumetric percent	Weight content
Cement	1	30	1
Liapor 1-4 mm	1	30	0.41
Liapor 4-8 mm	0.67	20	0.23
Sand < 2 mm	0.67	20	0.97
Water	-	-	0.57

Picture

Characteristic curve

Yielding element (first test series)

Test number: 1.10
Lab number: 5
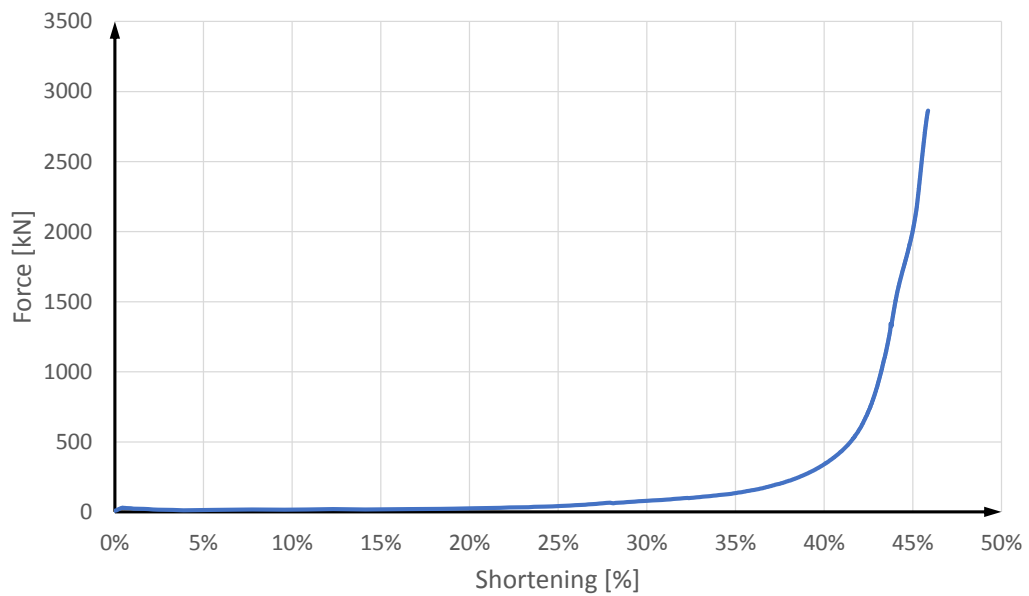Height: 400 mm
Type: TSR
Outer diameter: 165.1 mm
Comment: In this case a sheet iron pipe with a diameter of 120 mm and a wall thickness of 0.6 mm was used as lost formwork.

Mixture of filling

	Volumetric content	Volumetric percent	Weight content
Cement	1	30	1
Liapor 1-4 mm	1	30	0.41
Liapor 4-8 mm	0.67	20	0.23
Sand < 2 mm	0.67	20	0.97
Water	-	-	0.57

Picture

Characteristic curve

Dimensions

	outer diameter [mm]	inner diameter [mm]	wall thickness [mm]	height [mm]
outer pipe	130.0	128.8	0.6	200
inner pipe	120.0	118.8	0.6	200
total				390

Sketch
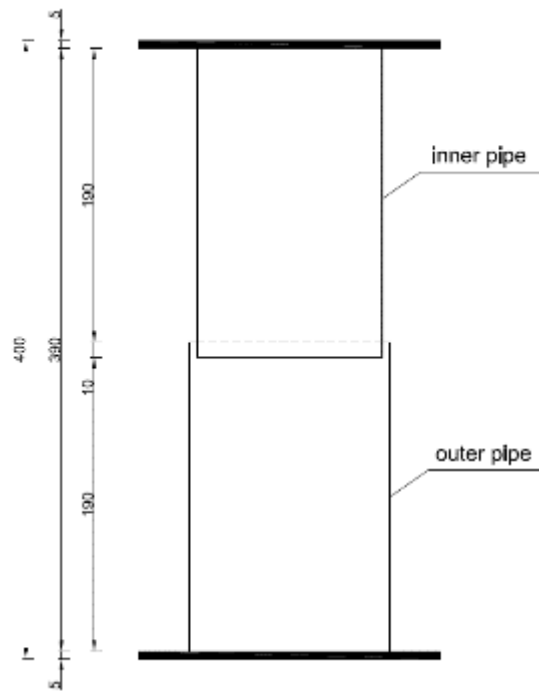
Picture

Yielding element (second test series)

Test number: 2.1
Lab number: 40/40/20 bl
Height: 400 mm
Type: TSR
Outer diameter: 130.0 mm
Comment: A sheet iron pipe was used for the inner and outer pipe.

Mixture of filling

	Volumetric content	Volumetric percent	Weight content
Cement	1	40	1
Liapor 4-8 mm	1	40	0.35
Sand < 2 mm	0.5	20	0.73
Water			0.40

Picture

Characteristic curve
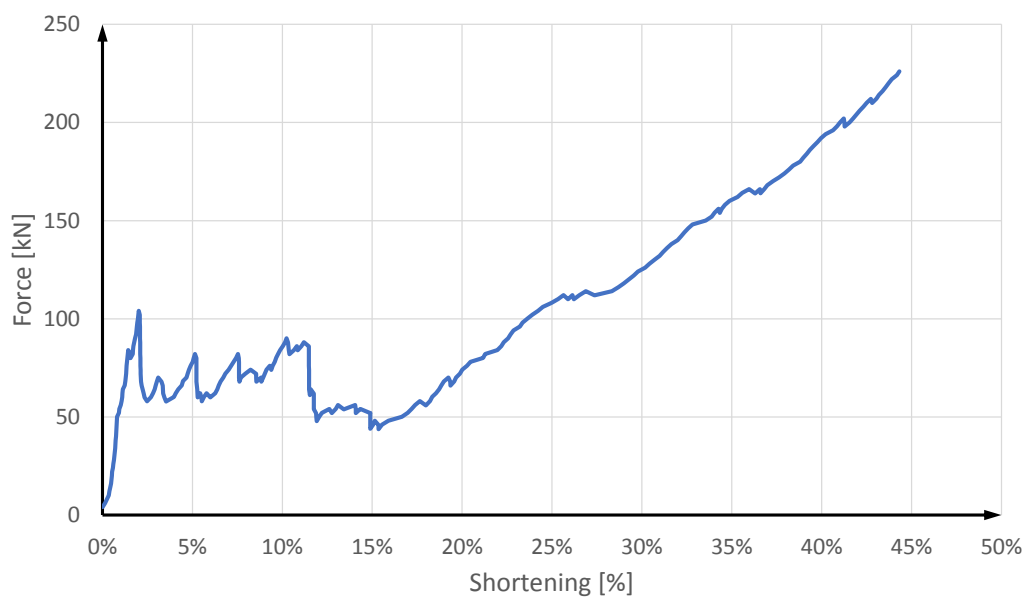
Dimensions

	outer diameter [mm]	inner diameter [mm]	wall thickness [mm]	height [mm]
outer pipe	134.0	130.0	2.0	200
inner pipe	124.0	120.0	2.0	200
total				390

Sketch
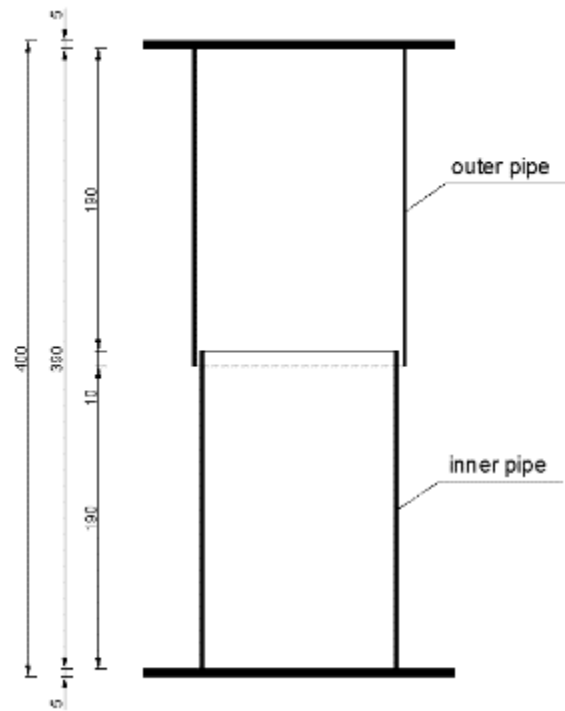
Picture

Yielding element (third test series)

Test number: 3.1
Lab number: 6
Height: 400 mm
Type: TSR
Outer diameter: 134.0 mm
Comment: Stove pipes with a hexagonal filling was used.

Mixture of filling

	Volumetric content	Volumetric percent	Weight content
Cement	1	20	1
Liapor 8-16 mm	3	60	0.98
Sand < 2 mm	1	20	1.46
Water	-	-	0.70

Picture

Characteristic curve

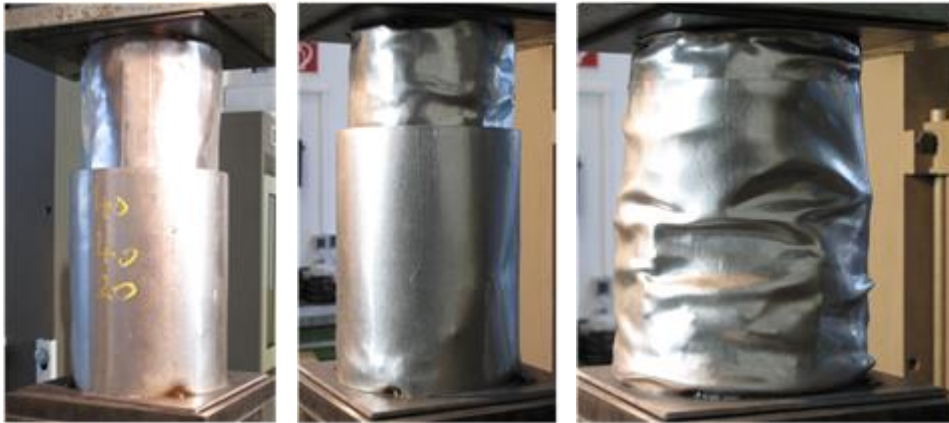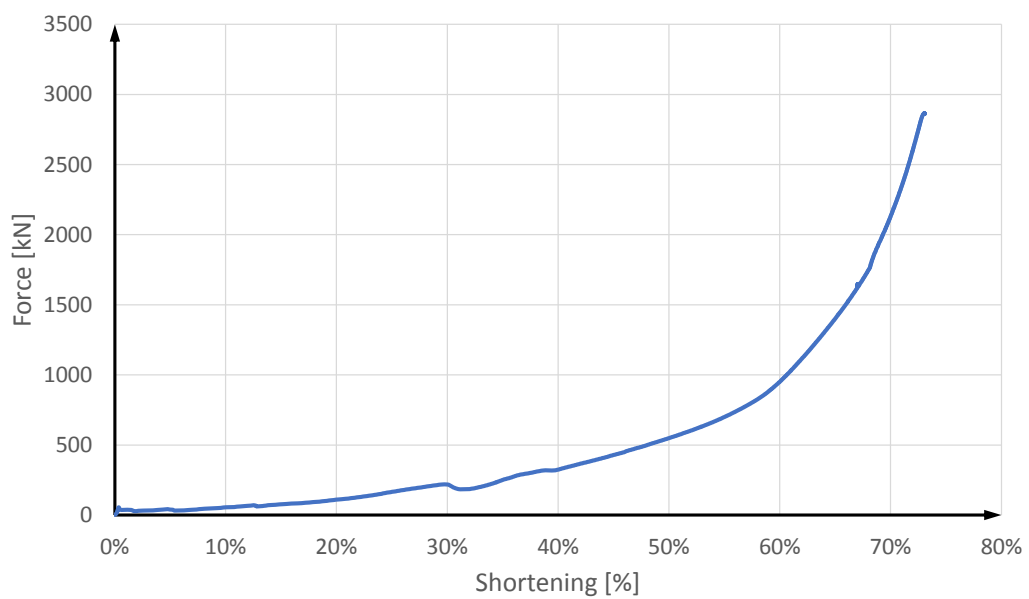## Yielding element (third test series)

Test number: 3.2
Lab number: 7
Height: 400 mm
Type: TSR
Outer diameter: 134.0 mm
Comment: A hexagonal filling with a centrically arranged steel pipe
(diameter: 25 mm, wall thickness: 0.6 mm) was used.

Mixture of filling

	Volumetric content	Volumetric percent	Weight content
Cement	1	30	1
Liapor 1-4 mm	1	30	0.41
Liapor 4-8 mm	0.67	20	0.23
Sand < 2 mm	0.67	20	0.97
Water	-	-	0.57

Picture

Characteristic curve

Yielding element (third test series)

Test number: 3.3
Lab number: 8
Height: 400 mm
Type: TSR
Outer diameter: 134.0 mm
Comment: In this case a sheet iron pipe with a diameter of 120 mm and a wall thickness of 0.6 mm
                    was used as lost formwork.

Mixture of filling

	Volumetric content	Volumetric percent	Weight content
Cement	1	30	1
Liapor 4-8 mm	1	30	0.35
Liapor 8-16 mm	0.67	20	0.22
Sand < 2 mm	0.67	20	0.97
Water	-	-	0.57

Picture

Characteristic curve
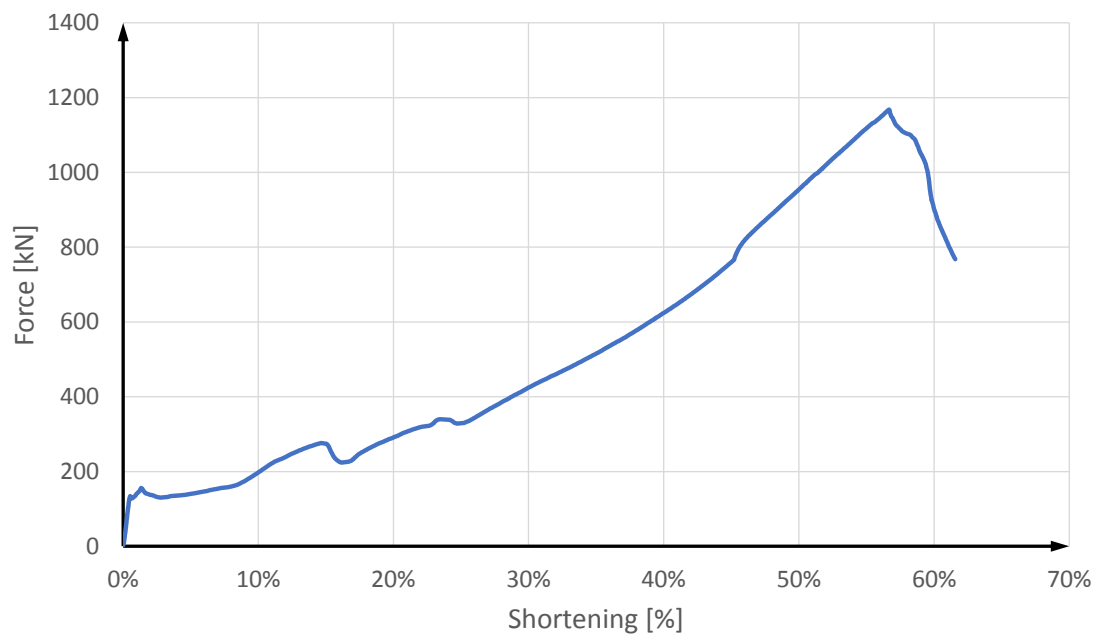
Dimensions

	outer diameter [mm]	inner diameter [mm]	wall thickness [mm]	Height [mm]
outer pipe	154.0	150.0	2.0	200
inner pipe	134.0	130.0	2.0	200
total				390

Sketch
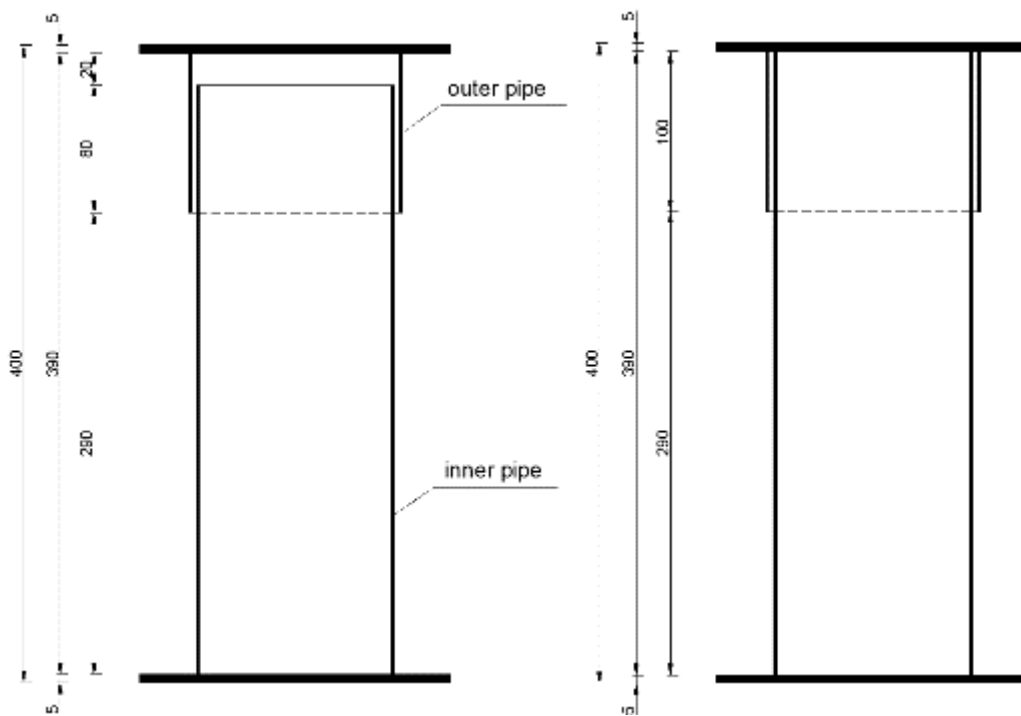
Picture

Yielding element (fourth test series)

Test number: 4.1
Lab number: 9
Height: 400 mm
Type: TSR
Outer diameter: 154.0 mm
Comment: In this test the filling is 2 cm longer than the inner pipe.

Mixture of filling

	Volumetric content	Volumetric percent	Weight content
Cement	1	40	1
Liapor 1-4 mm	0.75	30	0.31
Sand < 2 mm	0.75	30	1.09
Water	-	-	0.48

Picture

Characteristic curve

Yielding element (fourth test series)

Test number: 4.2
Lab number: 10
Height: 400 mm
Type: TSR
Outer diameter: 154.0 mm
Comment: In this test the filling is of equal length as the inner pipe.

Mixture of filling

	Volumetric content	Volumetric percent	Weight content
Cement	1	40	1
Liapor 1-4 mm	0.75	30	0.31
Sand < 2 mm	0.75	30	1.09
Water	-	-	0.48

Picture

Characteristic curve

Yielding element (fifth test series)

Test number: 5.1
Lab number: 11
Height: 400 mm
Type: TSR
Outer diameter: 154.0 mm
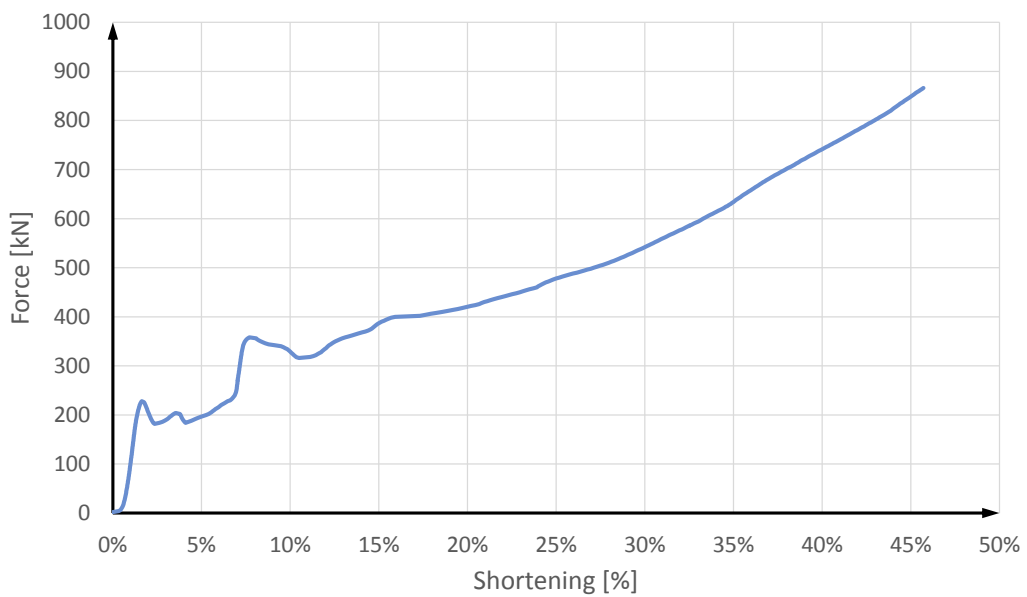Comment: In this test the filling is of equal length as the inner pipe. 2 cm of cork inlay was used.

Mixture of filling

	Volumetric content	Volumetric percent	Weight content
Cement	1	40	1
Liapor 1-4 mm	0.75	30	0.31
Sand < 2 mm	0.75	30	1.09
Water	-	-	0.48

Picture

Characteristic curve

Yielding element (fifth test series)

Test number: 5.2
Lab number: 12
Height: 400 mm
Type: TSR
Outer diameter: 154.0 mm
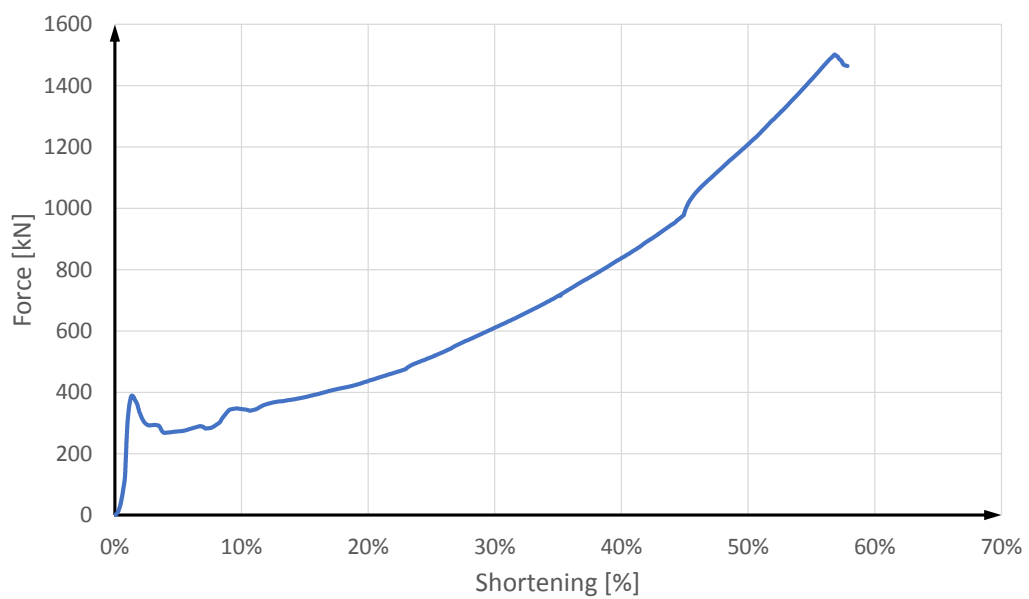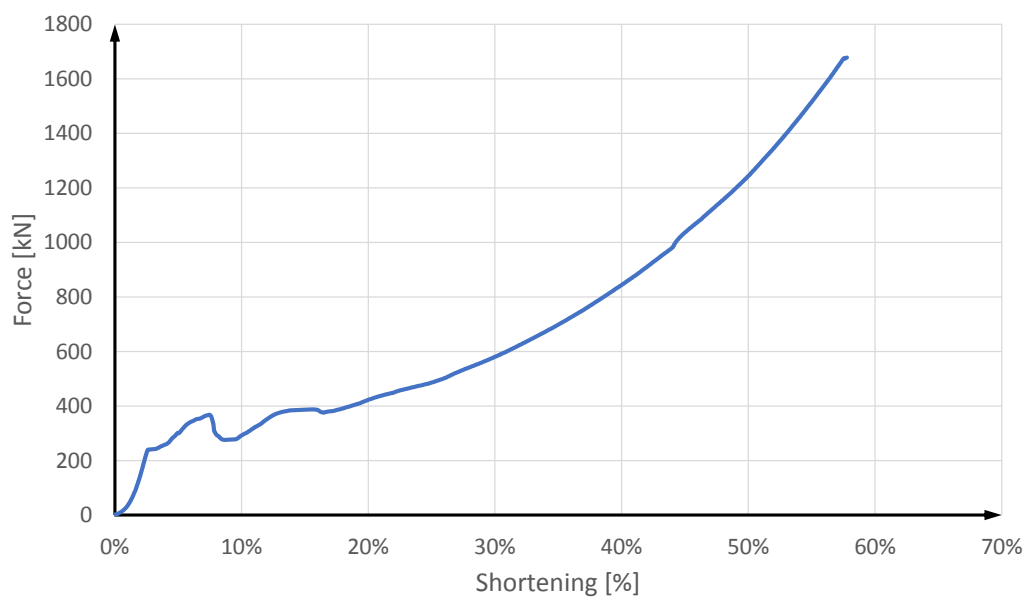Comment: In this test the filling is of equal length as the inner pipe. 2 cm of a soft elastic material was
                      was used.

Mixture of filling

	Volumetric content	Volumetric percent	Weight content
Cement	1	40	1
Liapor 1-4 mm	0.75	30	0.31
Sand < 2 mm	0.75	30	1.09
Water	-	-	0.48

Picture

Characteristic curve

Yielding element (fifth test series)

Test number: 5.3
Lab number: 13
Height: 400 mm
Type: TSR
Outer diameter: 154.0 mm
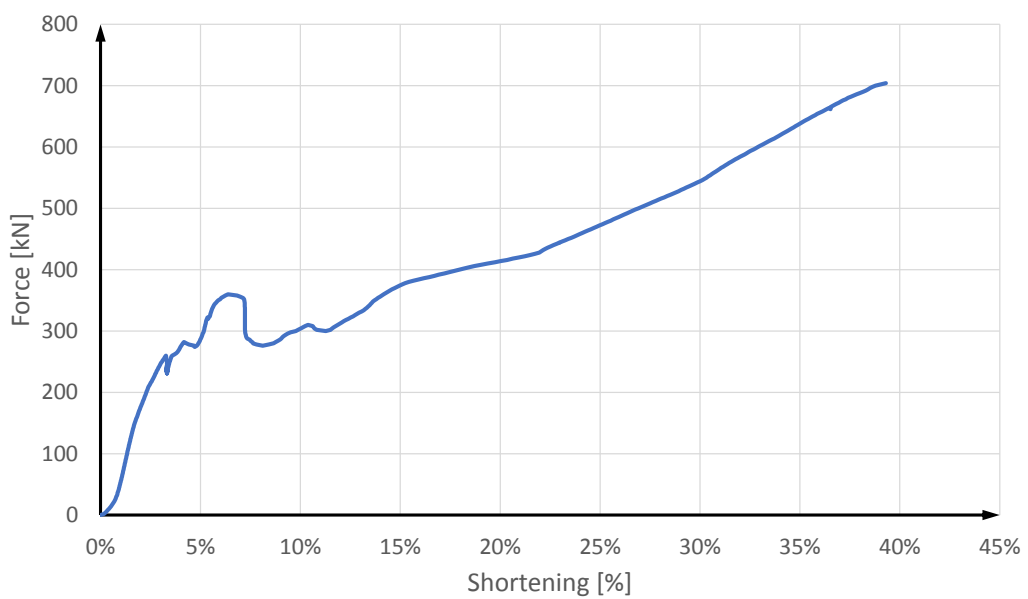Comment: In this test the filling is of equal length as the inner pipe. 2 cm of a soft elastic material was was used.

Mixture of filling

	Volumetric content	Volumetric percent	Weight content
Cement	1	40	1
Liapor 1-4 mm	0.75	30	0.31
Sand < 2 mm	0.75	30	1.09
Water	-	-	0.48

Picture

Characteristic curve

Yielding element (fifth test series)
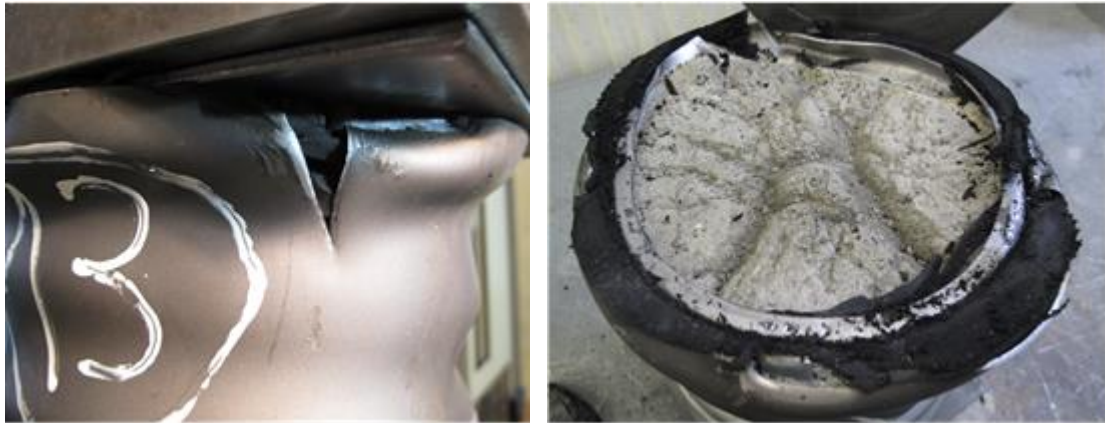
Test number: 5.4
Lab number: 14
Height: 400 mm
Type: TSR
Outer diameter: 154.0 mm
Comment: In this test the filling is of equal length as the inner pipe. 2 cm of a soft elastic material was
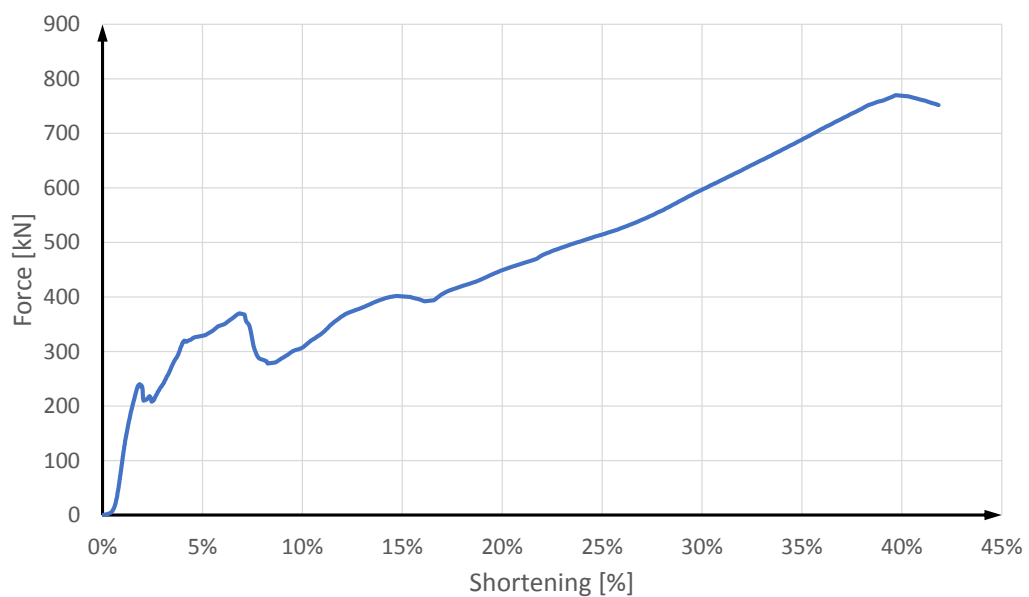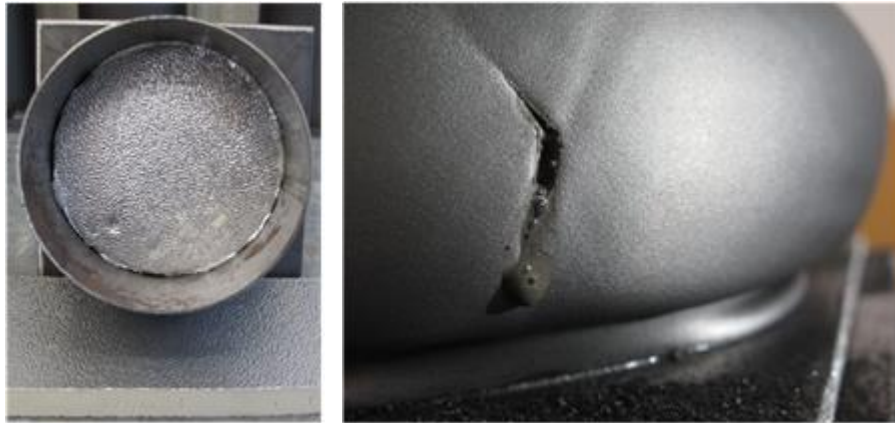   was used.

Mixture of filling

	Volumetric content	Volumetric percent	Weight content
Cement	1	40	1
Liapor 1-4 mm	0.75	30	0.31
Sand < 2 mm	0.75	30	1.09
Water	-	-	0.48

Picture

Characteristic curve

Yielding element (sixth test series)

Test number: 6.1
Lab number: 15
Height: 400 mm
Type: TSR
Outer diameter: 154.0 mm
Comment: A multi-perforated steel pipe was tested.

Mixture of filling
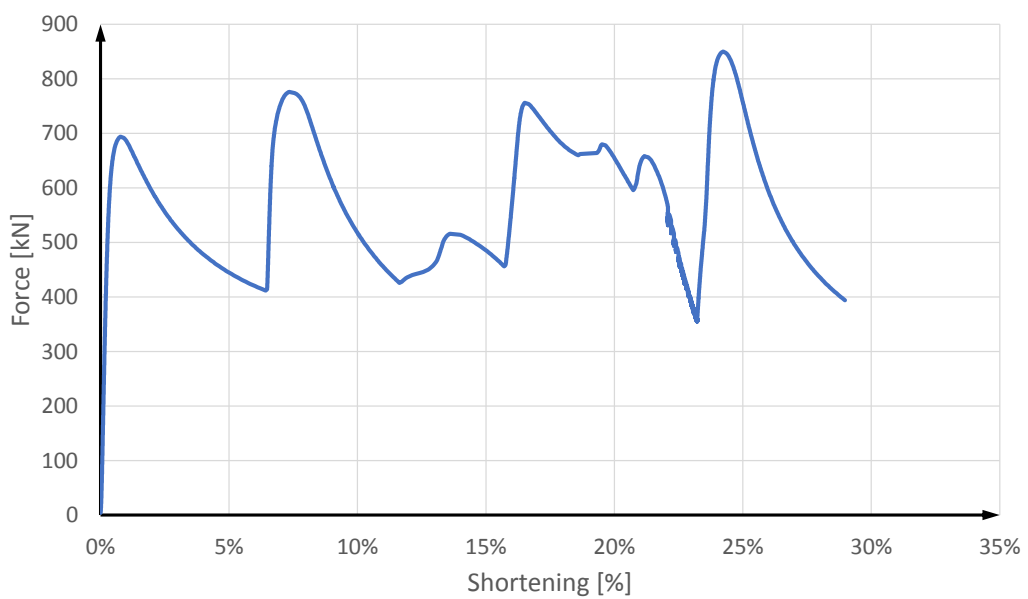
	Volumetric content	Volumetric percent	Weight content
Cement	1	40	1
Liapor 1-4 mm	0.75	30	0.31
Sand < 2 mm	0.75	30	1.09
Water	-	-	0.48

Picture

Characteristic curve

Appendix B

Determination of the depth of the failure zone and the deformation of a circular opening after Feder & Arwanitakis (1976)

Stresses around a circular opening for hydrostatic primary stress conditions:

$$\text{with } r = R_0 \rightarrow \sigma_r = p_a$$

$$\sigma_{r,pl} = (p_a + p_k)\left(\frac{r}{R_0}\right)^{\lambda_p - 1} \tag{2}$$

$$\text{with } r = \tilde{R} \rightarrow \sigma_r = \sigma_{r\tilde{R}}$$

$$\sigma_{r,pl} = (\sigma_{r\tilde{R}} + p_k)\left(\frac{r}{\tilde{R}}\right)^{\lambda_p - 1} - p_k \tag{3}$$

$$\lambda_p = \tan^2\left(45 + \frac{\varphi}{2}\right) \tag{4}$$

$$\lambda_{p,pl} = \tan^2\left(45 + \frac{\varphi_{pl}}{2}\right) \tag{5}$$

$$\lambda_{p,el} = \tan^2\left(45 + \frac{\varphi_{el}}{2}\right) \tag{6}$$

$$p_k = \frac{\beta_{gd}}{\lambda_p - 1} = c * \cot\varphi \tag{7}$$

$$p_{k,el} = \frac{\beta_{gd}}{\lambda_{p,el} - 1} = c_{el} * \cot\varphi_{el} \tag{8}$$

$$p_{k,pl} = \frac{\beta_{gd}}{\lambda_{p,pl} - 1} = c_{pl} * \cot\varphi_{pl} \tag{9}$$

$$\sigma_{\vartheta,pl} = \sigma_{r,pi} * \lambda_{p,pl} + p_{k,pl} * \left(\lambda_{p,pl} - 1\right) \tag{10}$$

$$\sigma_{r,pl} = \left(p_a + p_{k,pl}\right) * \left(\frac{r}{R_0}\right)^{\lambda_{p,pl} - 1} - p_{k,pl} \tag{11}$$

$$\sigma_{\vartheta\tilde{R}} = \left(p_i + p_{k,el}\right) * (1 - \sin\varphi_{el}) - p_{k,el} \tag{12}$$

$$\sigma_{r\tilde{R}} = \left(p_i + p_{k,el}\right) * (1 - \sin\varphi_{el}) - p_{k,el} \tag{13}$$

$$\tilde{R} = R_0 \left[\frac{2p_i - p_{k,el}(\lambda_{p,el} - 1) + p_{k,pl}(\lambda_{p,el} + 1)}{(p_a + p_{k,pl})(\lambda_{p,el} + 1)} \right]^{\frac{1}{\lambda_{p,pl}-1}} \tag{14}$$

$$\bar{R} = R_0 \left[\frac{p_i + p_{k,pl}}{\lambda_{p,pl}(p_a + p_{k,pl})} \right]^{\frac{1}{\lambda_{p,pl}-1}} \tag{15}$$

$$\sigma_{\vartheta,el} = {}^S pi \left[1 + \left(\frac{\tilde{R}}{r}\right)^2 \right] - {}^A pi \left[1 + 3\left(\frac{\tilde{R}}{r}\right)^4 \right] \cos 2\psi - \sigma_{r\tilde{R}} \left(\frac{\tilde{R}}{r}\right)^2 \tag{16}$$

$$\sigma_{r,el} = {}^S pi \left[1 + \left(\frac{\tilde{R}}{r}\right)^2 \right] - {}^A pi \left[1 - 4\left(\frac{\tilde{R}}{r}\right)^2 + 3\left(\frac{\tilde{R}}{r}\right)^4 \right] \cos 2\psi + \sigma_{r\tilde{R}} \left(\frac{\tilde{R}}{r}\right)^2 \tag{17}$$

Displacements in the elastic (pre-failure) zone:

$$r = \tilde{R} \rightarrow u_{\tilde{R}} = \tilde{R}(1 + v)\frac{p_i - \sigma_{\vartheta,\tilde{R}}}{E} \tag{18}$$

Displacements in the plastic (post-failure) zone:

$$\begin{aligned}
\frac{u_\infty}{r}\bigg|_{\substack{r < \tilde{R} \\ r > \bar{R}}} &= \frac{u_{\tilde{R}}}{r}\left(\frac{\tilde{R}}{r}\right)^{\alpha+1} + \frac{p_i}{E} * C_1 \left[\left(\frac{\tilde{R}}{r}\right)^{\alpha+1} - \left(\frac{r}{\tilde{R}}\right)^{\lambda_{p,pl}-1} \right] \\
&\quad * \left\{ 2 - \frac{p_{k,el}}{p_i}\left[\lambda_{p,el} - 1 - \frac{p_{k,pl}}{p_{k,el}}(\lambda_{p,el} + 1) \right] \right\} - \frac{p_i}{E} * C_2 \\
&\quad * \left[\left(\frac{\tilde{R}}{r}\right)^{\alpha+1} - 1 \right] * \left(1 + \frac{p_{k,el}}{p_i} * \frac{p_{k,pl}}{p_{k,el}} \right) \\
&= \boxed{\frac{u_{\tilde{R}}}{\tilde{R}}\left(\frac{\tilde{R}}{r}\right)^{\alpha+1} + \frac{p_i}{E} * K_u}
\end{aligned} \tag{19}$$

transformed

$$u_\infty = \boxed{\left(\frac{u_{\tilde{R}}}{\tilde{R}}\left(\frac{\tilde{R}}{r}\right)^{\alpha+1} + \frac{p_i}{E} * K_u \right) * r} \tag{20}$$

$$C_1 = \frac{1 - v * \lambda_{p,pl} + \alpha\left[\lambda_{p,el}(1 - v) - 2v\right]}{(\alpha + \lambda_{p,pl})(1 + \lambda_{p,el})} \tag{21}$$

$$C_2 = \frac{1 - v + \alpha(1 - 3v)}{\alpha + 1} \tag{22}$$

$$\frac{u_{\bar{R}}}{\bar{R}} = like\ formular(10), \qquad but\ with\ \boxed{r = \bar{R}} \tag{23}$$

$$\left.\frac{u}{r}\right|_{r < \bar{R}} = like\ formular\ (\ 10\ ), but\ with\ \boxed{\bar{R}, u_{\bar{R}}, \overline{K_u}, \overline{C_1}, \overline{C_2}}$$
$$instead\ of\ \boxed{\tilde{R}, u_{\tilde{R}}, K_u, C_1, C_2}$$

(24)

$$\overline{C_1} = \frac{1 - 2\nu * \lambda_{p,pl} + 2\alpha[\lambda_{p,pl}(1 - \nu) - \nu]}{(\alpha + \lambda_{p,pl})(1 + \lambda_{p,el})}$$

(25)

$$\overline{C_2} = \frac{1 - 2\nu + 2\alpha(1 - 2\nu)}{\alpha + 1}$$

(26)

Time- and load-dependent mechanical properties of the shotcrete liner after Schubert (1988)

$$\Delta\varepsilon_d = (\sigma_2\ C_{d\infty} - \varepsilon_d) * \left\{1 - e^{\frac{-\Delta C_{(t)}}{Q}}\right\}$$

(27)

$$\sigma_2 = \frac{\varepsilon_2 - \varepsilon_1 + \frac{\sigma_1}{E_{(t)}} + \varepsilon_d\left\{1 - e^{\frac{-\Delta C_{(t)}}{Q}}\right\} - \Delta\varepsilon_{sh}}{\frac{1}{E_{(t)}} + \Delta C_{(t)} + C_{d\infty}\left(1 - e^{\frac{-\Delta C_{(t)}}{Q}}\right)}$$

(28)

$$C_{(t)} = A\ t^{1/3}$$

(29)

$$E_{(t)} = E_{28}[(4.2 + 0.85\ t)/t]^{-0.5}$$

(30)

$$\varepsilon_{sh} = \varepsilon_{sh\ \infty} * t\ /\ (B + t)$$

(31)

Longitudinal displacement development after Panet & Guenot (1982)

$$u(x) = u_f + (u_\infty - u_f) * \left[1 - \left(\frac{0.84 * \tilde{R}}{x + 0.84 * \tilde{R}}\right)^2\right]$$

(32)

Pre-relaxation factor after Radončić (2011)

$$\frac{u_f}{u_\infty} = \frac{1}{3}e^{-0.15\frac{\tilde{R}}{r}}$$

(33)